



# NEW FRONTIERS IN CHEMISTRY

## New Front. Chem.

*(former Annals of West University of Timișoara – Series of Chemistry)*

*(2020) Volume 29, Number (Issue) 1, pp. 1-51*

*Ordinary Issue*

---

### TABLE OF CONTENTS

<b>Prediction of Biological Effects of Some Natural Sweeteners</b>	<b>1-11</b>
Denisa Ioana Voiculescu, Vasile Ostafe, Ciorsac Alecu, Adriana Isvoran	
<b>Obtaining Extracts from Morning Glory. Pharmacotoxicology</b>	<b>13-20</b>
Iacob Gabriel-Constantin, Duda Seiman Corina, Adina Negrea, Dan Marculescu	
<b>Characterization of Benzene and Coronene Molecules as Subsystems of a Graphene Nanoribbon in Different Bonding States</b>	<b>21-32</b>
Marina Alexandra Tudoran, Mihai V. Putz	
<b>Matriceal Heterojunctions on Graphene. First Metrological Measurements</b>	<b>33-51</b>
Doru Buzatu, Paula Svera (Ianasi), Mihai V. Putz	

PUBLISHER:  
 **Universitatea de Vest**  
din Timișoara



---

# NEW FRONTIERS IN CHEMISTRY: METADATA

---

*New Frontiers in Chemistry (New Front. Chem.)* is an open-access fee-free peer-review international academic journal addressing the modern trends and frontiers in fundamental, applicative and multidisciplinary chemistry, paralleling the ever-expanding chemical data, methods, and compounds available and continuously produced, towards cross fertilizing the multidisciplinary ideas as coming from Chemistry combined with Mathematics, the Natural and Applied sciences (Physics, Biology, Medicine, Agriculture, Environmental, Engineering), and beyond.

---

**NEW FRONTIERS IN CHEMISTRY**  
**(NEW FRONT. CHEM.)**  
is published biannually by

**West University of Timișoara**  
Blvd. V. Parvan 4  
Timisoara 300223, ROMANIA  
E-mail: [newfrontchem@iqstorm.ro](mailto:newfrontchem@iqstorm.ro)  
Web: [www.newfrontchem.iqstorm.ro](http://www.newfrontchem.iqstorm.ro)

ISSN 2668-9189  
ISSN-L 2393 – 2171

### Subscription Price per Volume

Electronic: open access    Print: on demand by above email address

---

Additional color graphics is available in the e-version of this Journal

---

Copyright © 2020 West University of Timișoara. Printed in Romania. Submission to publication implies authors have the right to assign the copyright for publication herein contained, and no right protected by copyright to their works have been previously assigned; Acceptation for publication implies that authors' works contain no matter that is libelous or is otherwise unlawful or that invades individual privacy or infringes any proprietary right or any statutory copyright; Publication implies the material is original (at least 50% updated or syntheses of previously published – appropriately cited – works are considered original); authors agree to indemnify and hold the Publisher harmless against any claim or judgment to the contrary; authors (and all coauthors) have the right to present orally in any forum all or part of their works. The Publisher, as copyright owner upon (e-)publication has authority to grant permission to reproduce the papers. The Publisher assumes no responsibility for any statements or fact or opinion expressed in the published papers.

---

# NEW FRONTIERS IN CHEMISTRY: EDITORS

---

*Editor-in-Chief:*

*(and Editorial Office of New Front. Chem.)*

**MIHAI V. PUTZ**

West University of Timișoara (WUT)

Faculty of Chemistry, Biology, Geography (CBG)

Biology-Chemistry Department

Laboratory of Computational and Structural Physical-Chemistry for  
Nanosciences and QSAR

Pestalozzi Street No.16, Timișoara, RO-300115

ROMANIA

Phone: +40-256-592638, Fax: +40-256-592620

Ems: [mihai.putz@e-uvv.ro](mailto:mihai.putz@e-uvv.ro), [mv\\_putz@yahoo.com](mailto:mv_putz@yahoo.com)

*Senior Editor:*

**VASILE OSTAFE**

West University of Timișoara

Faculty of Chemistry, Biology, Geography

Biology-Chemistry Department

Timișoara, ROMANIA

Ems: [vasile.ostafe@e-uvv.ro](mailto:vasile.ostafe@e-uvv.ro), [vostafe@yahoo.com](mailto:vostafe@yahoo.com)

**Editorial Board:**

**OTTORINO ORI**

Actinium Chemical Research  
Head of Nanochemistry Division  
Rome, ITALY

**ALINA ZAMFIR**

University of Arad  
Department of Chemistry and Biology  
Arad, ROMANIA

**MIRCEA V. DIUDEA**

“Babes-Bolyai” University of Cluj-Napoca  
Faculty of Chemistry and Chemical Engineering  
Department of Organic Chemistry  
Cluj-Napoca, ROMANIA

**JOEL F. LIEBMAN**

University of Maryland, Baltimore County (UMBC)  
The Department of Chemistry and Biochemistry  
Baltimore (MD), USA

**FRANCESC MAS**

University of Barcelona  
Departament de Química Física  
SPAIN

**LIONELLO POGLIANI**

Universitat de València  
Facultat de Farmàcia  
Unitat d'Investigació en Disseny de Farmacs i Connectivitat Molecular  
SPAIN

**MARILENA FERBINTEANU**

University of Bucharest  
Faculty of Chemistry  
Inorganic Chemistry Department  
ROMANIA

**SPERANTA AVRAM**

University of Bucharest  
Faculty of Biology  
Department of Anatomy, Animal Physiology and Biophysics  
ROMANIA

**FRANCO CATALDO**

Actinium Chemical Research  
General Director  
Rome, ITALY

**EUGENIA FAGADAR-COSMA**

Institute of Chemistry Timisoara of Romanian Academy  
Timisoara, ROMANIA

**FRANCISCO TORRENS**

Universitat de València  
Institut Universitari de Ciència Molecular  
SPAIN

**NAZMUL ISLAM**

Techno Global-Balurghat  
Conceptual and General Chemistry  
INDIA

**MARGHERITA VENTURI**

University of Bologna  
Dipartimento di Chimica «Ciamician»  
Bologna, ITALY

**IONEL MANGALAGIU**

University Alexandru Ioan Cuza of Iasi  
Organic Chemistry Department  
Iași, ROMANIA

**RADIVOJE PRODANOVIC**

University of Belgrade  
Department of Biochemistry  
SERBIA

**KATHLEEN SWALLOW**

Emeritus at Merrimack College  
Department Analytical Chemistry  
USA

**LÁSZLÓ ALMÁSY**

Hungarian Academy of Sciences  
Wigner Research Centre for Physics  
Budapest, HUNGARY

**Advisory Editors**

*(from active members of Biology-Chemistry Department and of Doctoral School of Chemistry of West University of Timișoara):*

VASILE OSTAFE (Biochemistry, Chromatography, Environmental Chemistry)  
IONEL CIUCANU (Instrumental Techniques for Analytical Chemistry)  
ADRIANA ISVORAN (Biophysics, Bioinformatics)  
MIHAI V. PUTZ (Nanochemistry, Quantum Chemistry)  
TITUS VLASE (Thermal Analysis, Chemical Kinetics, Chemistry of Solid State)  
GABRIELA VLASE (Inorganic Chemistry, Thermal Analysis)  
GABRIELA PREDA (Organic Chemistry, Catalysis)  
CONSTANTIN BOLCU (Organic Chemistry, Polymers)  
VLAD CHIRIAC (General and Analytical Chemistry, Electrochemistry)  
DANA VLASCICI (Analytical Chemistry)  
DANIELA DASCALU (Thermodynamics and Chemical Statistics)  
CORINA DUDA-SEIMAN (QSAR, Organic Chemistry, Medicinal Chemistry)  
LAURA PITULICE (Environmental Chemistry)  
BEATRICE VLAD-OROS (Chemical and Enzyme Kinetics)  
NICOLETA IANOVIC (Aerobiology, Plant Physiology)

**Honorary Editors**

*(as Doctor Honoris Causa of WUT/CBG & Formers Editors and Developers of Annals of West University of Timișoara – Series Chem.):*

ALEXANDRU BALABAN (Texas A&M University at Galveston, USA, & Romanian Academy, Romania)  
HAGEN KLEINERT (Berlin Free University, Germany)  
KATLEEN SWALLOW (Merrimack College, USA)  
GABOR NÁRÁY-SZABÓ (“Lorand Eötvös” University Budapest, Hungary)  
MARIUS ANDRUH (Romanian Academy, Bucharest)  
VASILE OSTAFE (West University of Timisoara, Romania)  
VICTOR EMANUEL SAHINI (†, Polytechnic Bucharest, Romanian Academy, Romania)  
EUGEN SEGAL (†, University of Bucharest, Romanian Academy, Romania)  
ZENO SIMON (†, Romanian Academy, Romania)  
ADRIAN CHIRIAC (†, West University of Timisoara, Romania)  
MIRCEA MRACEC (†, West University of Timisoara, Romania)  
NICOLAE BONCIOCAT (†, Babes-Bolyai University, Cluj-Napoca, Romania)  
ALAN R. KATRITZKY (†, University of Florida, Gainesville, USA)

Article

## PREDICTION OF BIOLOGICAL EFFECTS OF SOME NATURAL SWEETENERS

*Denisa Ioana Voiculescu*<sup>1,2</sup>, *Vasile Ostafe*<sup>1,2</sup>, *Ciorsac Alecu*<sup>3</sup>,  
*Adriana Isvoran*<sup>1,2\*</sup>

<sup>1</sup> West University of Timisoara, Department of Biology-Chemistry, 16 Pestalozzi,  
300115 Timisoara, Romania

<sup>2</sup> West University of Timisoara, Advanced Environmental Research Laboratories, 4  
Oituz, 300086 Timisoara, Romania

<sup>3</sup> Politehnica University of Timișoara, Department of Physical Education and Sport, 2  
Piata Victoriei, 300006 Timișoara, Romania

### ABSTRACT

This study presents predictions concerning the pharmacokinetics and biological effects of the most commonly used natural sweeteners. Investigated sweeteners have favorable pharmacokinetic profiles as they are not able to affect the central nervous system, are not considered as inhibitors of the cytochromes P450 that are involved in the metabolism of xenobiotics and have not the ability to penetrate the skin. Our results also reveal some possible side effects of natural sweeteners: hyperuricemia, acidosis, hematotoxicity, cyanosis and toxicity through respiration. These data sustain that much more research is needed to fully understand the biological effects of dietary natural sweeteners in humans.

**Keywords:** sweeteners, biological effects, pharmacokinetics;

### 1. INTRODUCTION

Sweeteners are used in numerous food processes, and the effect of the ingesting of these kinds of compounds may affect health status and microbiota composition [1]. They are considered sugar alternatives that mimic the sweet taste of sugar but have an insignificant impact on energy intake [2].

---

\* Correspondent author: +40256592634; Fax:+40256592620, E-mails: adriana.isvoran@e-uvt.ro

When people consume sweet foods, the taste buds receive different impulses and their response is different from one sweetener to another. The interactions that they form in the buccal cavity stimulate the brain through the neurons. The sensation of sweetness depends on the dextrogyre conformation of the sweetener that is why D-glucose is sweet, and L-glucose emanates a salty taste.

Sweeteners are often found in food ingredients and they are recommended for consumption, examples of commercial foods where we find the most common sweeteners being sweets, juices, sauces, chewing gum [3]. Sweeteners are also found in pharmaceutical preparations and drugs as excipients, the pharmaceutical industry uses lactose and saccharose as inactive ingredients of drugs tablets because of their compressibility properties. [4,5]. The effects of sweeteners on the organism can be toxic and lead to oxidative stress and allergies [6]. Furthermore, it is considered that by reducing the number of sweeteners in food, people would prevent diseases like caries, diabetes and obesity [2].

From the point of view of origin, the sweeteners are divided into two groups: natural and synthetic, the natural ones being glycosidic or non-glycosidic. To be accepted on the market, the natural sweeteners must have a good taste and not be toxic, and for this, that compound has to be soluble in aqueous solutions. Besides this, their price must be acceptable for the majority of consumers. The most common natural sweeteners are sucrose (a disaccharide formed from units of glucose and fructose), maltose (another disaccharide made from two units of glucose), lactose (the disaccharide made from one unit of glucose and one of galactose) and the monosaccharides, among glucose and fructose are the most familiar (Figure 1). Galactose is a monosaccharide similar to glucose and fructose, but the three molecules have distinct stereochemistry [7].

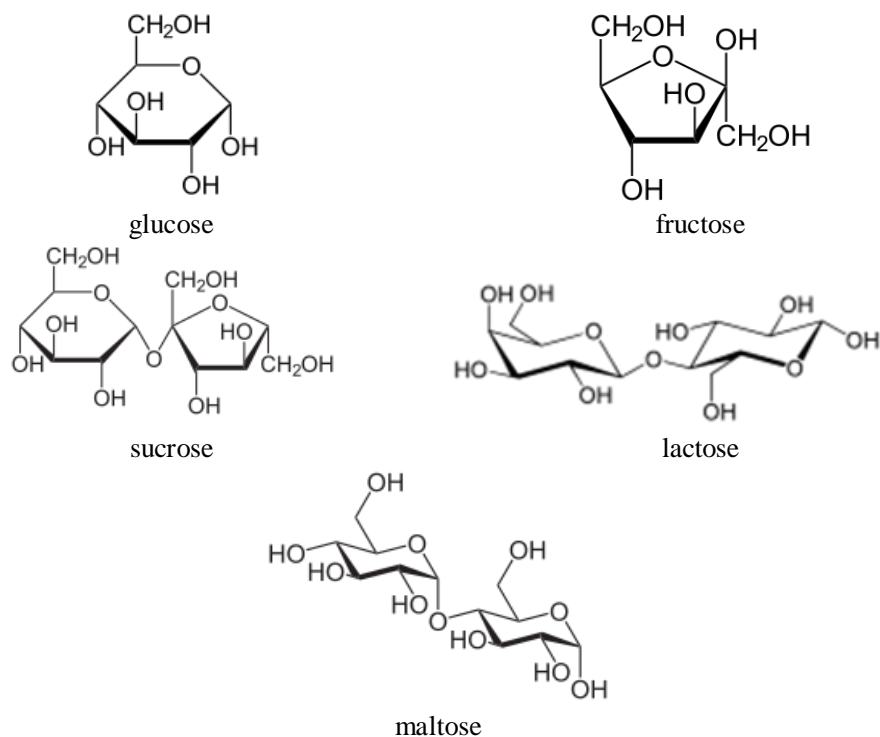


Figure 1. Structural formulas of the most common natural sweeteners

Many foods and drinks we consume every day have added natural sweeteners. Scientific literature data reveal some biological effects of these natural sweeteners, especially eating disorders and obesity [8]. Sucrose, used as the source of sugar, conducted to important effects on eating motivation and preferences [9] and some addictive effects [10]. Glucose intake have shown suppression of feeding [11], can induce oxidative stress, activates protein kinase C, endorses the formation of advanced glycation end-products, enhances hexosamine biosynthetic pathway and alters gene expressions [12]. Furthermore, high glucose intake contributes to the development of insulin resistance and dysfunction of insulin secretion, mediates irreversible cell damage and encourages the proliferation of cancer cells, potentiates a suitable environment for infections and conducts to development of osteoarthritis [12]. Other studies revealed that fluctuations in glucose levels have a negative metabolic impact on *Diabetes mellitus* and might impact the development of complications [13]. Fructose is considered by humans sweeter than glucose, fructose sweetness being perceived earlier than that of sucrose or glucose [14]. Like glucose, fructose might also induce modifications in eating motivation and eating disorders [8,15]. High consumption of fructose has been associated to prevalence of metabolic diseases (dyslipidemia, insulin resistance, hepatic steatosis and nonalcoholic fatty liver diseases, high blood pressure) effects on the gut microbiota conducting to impairment in intestinal mucosa integrity [16].

A high fructose intake may also induce advanced glycation end-products accumulation in the liver causing lipogenesis and intracellular lipids deposition conducting to a proinflammatory response [16]. Galactose intake is linked with the risk of ovarian cancer [17], oxidative stress, hormonal disturbances and spermatotoxic effect [7]. Maltose is the major product resulting from starch digestion by the enzyme beta-amylase (SAPHIRO et al, [18]). Some people manifest lactose intolerance meaning that they are not able to break lactose into its constituents because of insufficient lactase production. People characterized by lactose intolerance may experience allergic reactions, pain, bloating or swelling of the abdomen, diarrhea, nausea, production of gas [5].

Most of the studies revealing the effects of the investigated sweeteners have been performed in rodents, being considered that they display anatomical and physiological similarities to humans [19], but the transfer of information obtained through animal tests to humans strongly depends on the ability to measure the same endpoints in animals. Considering the expenses and the ethical concerns on using both animals and humans for testing purposes, the role of computational approaches in hazard assessment turns out to be recognized. The quantity and variety of data obtained through experimental toxicity studies permitted the building of truthful models and tools for computational toxicology assessment. Computational approaches are recognized by the Organization of Economic and Co-operation Development (OECD) [20] and European Food Safety Association [21] and are regularly used in assessing the toxicological effects of various chemicals on humans [22-29].

Taking into account the lack of data concerning the human health effects of the most used natural sweeteners (glucose, fructose, galactose, sucrose, lactose, maltose), the aim of this study is to use a computational approach to assess their biological effects on humans.

## 2. METHOD

Specific literature is abundant in computational tools available for predicting the biological effects of various types of chemicals. These tools are used to predict, analyze, simulate and/or visualize the biological and or side effects of chemicals. The outcomes of the computational methods object to complement and/or guide toxicity tests and prioritize chemicals. We have selected for this study SwissADME [30] and PASS [31] free accessible online computational tools, that are also robust and continuously updated and have the accuracy of predictions higher than 70%.

In the computational assessment of the biological activity of chemical compounds, predictions are usually based on the analysis of molecular properties (descriptors of chemicals) as there is a supposed relationship between chemical structures and biological activity in a chemical dataset [32]. As an example, the most used rule for predicting the oral bioavailability of chemical compounds is Lipinski's rule. It states that a compound with good oral bioavailability must meet the following criteria: molecular weight (MW) must be less than 500 daltons, the octanol-water partition coefficient (logP) must not exceed 5, there are not more than 5 hydrogen bond donors (HBD) and no more than 10 hydrogen bond acceptors (HBA) [33]. In this study, the ZINC database (<https://zinc.docking.org/>) was used to extract the SMILES (Simplified Molecular Input Line Entry System) formulas, the structural data file files (sdf) and the physical-chemical properties of the considered compounds. ZINC database contains information concerning 230 million chemical compounds that are commercially available and can be used in particular for molecular docking studies. This base can be accessed free of charge, is available online [34].

SwissADME (<http://www.swissadme.ch/>) software was used to obtain information concerning the pharmacokinetics of investigated sweeteners used in the food industry. It is a freely available web tool that allows the computation of the physicochemical properties of a chemical compound and its pharmacokinetic profile starting from the SMILES formula. The accuracy of predictions of SwissADME tools is situated between 72% and 94%. It supports studies that led to the discovery of new drugs, predicts interactions between various types of molecules, such as interactions between proteins and ligands, between human cytochromes and their inhibitors and between the glycoprotein P and its substrates. This software also predicts interactions between molecules and the body, i.e intestinal absorption and blood-brain barrier penetration) [35].

Prediction of Activity Spectra of Substances (PASS) is another software free available online (<http://www.pharmaexpert.ru/passonline/>) that has been used to obtain predictions concerning the side effects of investigated sweeteners [36]. PASS is a computational tool allowing prediction of biological activity and/or toxic and side effects of a chemical compound starting from its SMILES formula with a mean accuracy of prediction about 90%. PASS computational tool independently estimates two probabilities: the probability that the investigated compound belongs to a particular class of active compounds (Pa) or inactive compounds (Pi). The value of Pa is computed taking into account the similarity of the molecule under investigation with the structures of those molecules within the training set which are the most typical in a subset of "actives". Consistently, Pi reflects the similarity of the investigated compound with the molecules within the training set that belongs to the subset of "inactive". Activities with Pa>Pi are considered as promising for a given compound and a good accuracy of prediction is obtained for Pa>0.7.

All these methods have been developed for predicting the biological activity and/or side effects of drug candidates, but they were successfully applied for other chemicals: water-soluble derivatives of chitosan [23], cosmetic ingredients [26], parabens [25], steroids [24], pesticides [26]; [27], oligosaccharides [28].

### 3. RESULTS AND DISCUSSIONS

Taking into account the importance of the molecular properties for the biological activity of chemicals, the physicochemical properties of the sweeteners under investigation are extracted from ZINC database and are presented in Table 1. This table contains molecular descriptors related to the molecule dimension expressed by the molecular weight (MW), to polarity such as H-bond donors (HBD), H-bond acceptors (HBA) and topological polar surface area (TPSA), to electric charge, to lipophilicity expressed by partition coefficient (logP) and to flexibility expressed by the number of rotatable bonds (NRB) of the molecule.

**Table 1:** Physical and chemical proprieties of investigated carbohydrates extracted from ZINC Database: logP (partition coefficient), HBD (number of H bonds donor), HBA (number of H bonds acceptors), TPSA (polar topological area), MW (molecular mass), NRB- number of rotatable bonds

Compound	logP	HBD	HBA	Net charge	TPSA (Å <sup>2</sup> )	MW (g/mol)	NRB
Glucose	-3.22	5	6	0	110	180.15	2
Fructose	-2.04	5	6	0	110	180.15	2
Galactose	-2.64	5	6	0	110	180.15	5
Sucrose	-3.75	8	11	0	190	342.29	5
Lactose	-3.43	8	11	0	189	342.29	4
Maltose	-4.45	8	11	0	190	342.29	4

Compounds having a small molecular weight, increased lipophilicity (high value for logP) and reduced flexibility (low number of rotatable bonds) are considered to have a better membrane permeation and a good oral absorption [36].

Data presented in Table 1 illustrate that all of these compounds are hydrophilic and expose a high topological polar area, are not charged, have low molecular weight and reduced flexibility as the number of rotatable bonds is low. Monosaccharides totally respect the Lipinski's rule and theoretically have ideal oral bioavailability as their physicochemical parameters are associated with acceptable aqueous solubility and intestinal permeability. Disaccharides illustrate a high number of hydrogen bonds donors and acceptors, correlated to their increased TPSA and leading to poor permeability across the membrane bilayer.

The pharmacokinetic properties of the studied sweeteners have been obtained using SwissADME software and are presented in Table 2.

All investigated sweeteners illustrate poor gastrointestinal absorption and are considered as substrates of the P-gp protein, emphasizing that their systemic exposure is reduced. The poor absorption of disaccharides is correlated with the fact that they cannot cross the mucosa, they are hydrolyzed into monosaccharides. The glucose is able to cross the enterocytes and to reach the hepatic portal system. The fructose and the galactose are converted to glucose, being metabolized only in this form [13].

It is worth mentioning that the calculations of the probabilities of gastrointestinal absorption, or bioavailability are done without taking into account the fact that the cells have special transporters for certain molecules, such as for glucose (and the other monosaccharides). By means of these transporters, the speed of entry into the cells of the studied molecule is significantly higher than the simple passage (diffusion) through the biological membranes. In reality, the bioavailability of glucose and the rate of entry into cells is much higher than was calculated based on the descriptions used by the prediction software mentioned above.

**Table 2:** Pharmacokinetic properties of the studied sweeteners: GI- gastrointestinal absorption, BBB- blood-brain barrier penetration, P-gp – P-glycoprotein, CYP- cytochrome P450, LogKp- coefficient of passage through the skin

Com pound	GI	BBB	P-gps	Inhibition of				
				CYP1A2	CYP2C19	CYP2C9	CYP2D6	CYP3A4
Glucose	Low	no	yes	no	no	no	no	no
Fructose	Low	no	yes	no	no	no	no	no
Galactose	Low	no	yes	no	no	no	no	no
Sucrose	Low	no	yes	no	no	no	no	no
Lactose	Low	no	yes	no	no	no	no	no
Maltose	Low	no	yes	no	no	no	no	no

Investigated carbohydrates are not capable of penetrating the blood-brain barrier. It is not an unexpected result as it is known that the additive effect of increasing TPSA (through increase in HBA/HBD count) on decreasing passive permeability and simultaneously increasing P-gp transport efficiency is responsible for a decrease in the chemical exposure in the brain [37]. However, glucose is the essential energy substrate for the brain and supports the energy requirements of the central nervous system function, but it enters brain cells through glucose transporters [13]. It is also known that disaccharides are not able to reach the blood circulation (unless they are injected) and consequently, the predictions concerning the blood barrier penetration are not necessary for these compounds. It underlines one of the limitations of the *in silico* tools that allow to test any molecule even for improbable biological actions and the significant role of the researchers in interpreting these predictions.

None of these sweeteners is an inhibitor of the human cytochromes and it reveals that they do not interfere with co-administrated drugs.

Figure 1 shows the logarithmic value (logKp) of the skin penetration coefficient. All the natural sweeteners considered in this study have low values of logKp, thus illustrating their reduced ability to penetrate through the skin. This result is important for people working in the factories where these sweeteners are produced and / or packaged because they are professionally exposed.

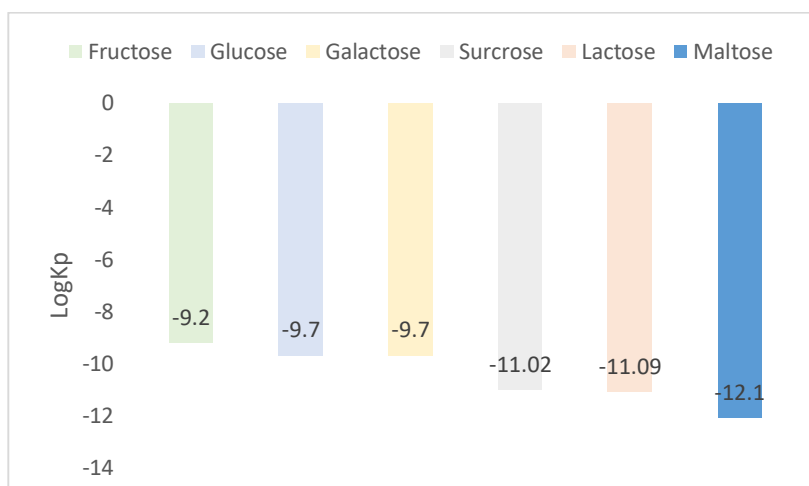


**Figure 1.** Logarithmic values of the skin penetration coefficients for investigated sweeteners

The use of PASS online software concerning the side effects of investigated sweeteners are illustrated in table 3.

**Table 3.** Predictions obtained using PASS software concerning the side effects of investigated sweeteners

Compound	Predicted side effects and the probability for every prediction
Glucose	Hyperuricemia (0.936), weight loss (0.930), acidosis (0.924), toxic by respiration (0.916)
Fructose	Hyperuricemia (0.778), hematotoxic (0.766), ulcer (0.760)
Galactose	Hyperuricemia (0.936), weight loss (0.930), acidosis (0.924), toxic by respiration (0.916)
Sucrose	Hyperuricemia (0.943), acidosis (0.931)
Lactose	Cyanosis (0.927), toxic by respiration (0.931), weight loss (0.917), acidosis (0.920), hyperuricemia (0.909), hematotoxic (0.905)
Maltose	Cyanosis (0.927), toxic by respiration (0.931), weight loss (0.917), acidosis (0.920), hyperuricemia (0.909), hematotoxic (0.905)

Data presented in Table 3 reveal common side effects of investigated sweeteners: hyperuricemia, acidosis, hematotoxicity, lactose and maltose illustrating the higher number of possible side effects. Some of these effects have already been noticed. High fructose intake may conduct to developing metabolic disease [38] and hyperuricemia [39] and fructose, lactose, sucrose and maltose may produce acidosis [40]. Another study revealed that galactose consumption as the only carbohydrate source promotes fat loss [41].

It is commonly known that intake of sweeteners conducts to weight gain, and it is surprising to notice that some of the investigated sweeteners may produce weight loss. A high concentration of any of investigated sweeteners in blood conducts to acidosis that further may produce weight loss. It illustrate that weight loss is a consequence of acidosis, not of the intake of sweeteners. Moreover, these predictions concern the situation of the intake of only the

sweeteners, not in combination with other compounds of diet. These results underline other limitation of computational assessment of biological effects of chemicals, these predictions do not take into account the quantity of ingested chemicals and the interactions with other compounds of the diet.

#### 4. CONCLUSION

The results obtained within this work show that the investigated sweeteners have favorable pharmacokinetic profiles as they are not able to affect the central nervous system, are not considered as inhibitors of the cytochromes P450 that are involved in the metabolism of xenobiotics and have not the ability to penetrate the skin. The results envisaging the poor ability of natural sweeteners to penetrate the skin are important for those who work in factories that produce, pack or use these sweeteners because they are professionally exposed and can be contaminated with larger quantities of these compounds and the adverse biological effects can be pronounced.

Our results also reveal some possible side effects of natural sweeteners: hyperuricemia, acidosis, hematotoxicity, cyanosis and toxicity through respiration. Literature data reveal that only hyperuricemia and acidosis have been observed, but we must take into consideration their other possible side effects. Our data sustain that much more research is needed to fully understand the biological effects of dietary natural sweeteners in humans.

#### REFERENCES

1. Ruiz-Ojeda F.J.; Plaza-Díaz.; Sáez-Lara M.J.; Gil A. Effects of Sweeteners on the Gut Microbiota: A Review of Experimental Studies and Clinical Trials. *Adv Nutr* **2019**, *10*, 31–48. Doi:10.1093/advances/nmy037.
2. Lohner S.; Toews I.; Meerpohl J.J. Health outcomes of non-nutritive sweeteners: analysis of the research landscape. *Nutr J* **2017**, *16*:55. Doi: 10.1186/s12937-017-0278-x.
3. Das A.; Chakraborty R. An Introduction to Sweeteners. In: Merillon JM., Ramawat K. (eds) Sweeteners. *Reference Series in Phytochemistry*. Springer, Cham **2016**, 1-13. Doi: [https://doi.org/10.1007/978-3-319-26478-3\\_1-1](https://doi.org/10.1007/978-3-319-26478-3_1-1).
4. Balbani A.P.S.; Stelzer L.B.; Montovani J.C. Pharmaceutical excipients and the information on drug labels, *Rev. Bras. Otorrinolaringol.* **2006**, *72*, 3:400. Doi: <http://dx.doi.org/10.1590/S0034-72992006000300018>.
5. Banas A.; Banas K.; Kalaiseveli S.M.P.P.; Pawlicki B.; Kiwatek W.M.; Breese M.B.H. It is possible to find presence of lactose in pharmaceuticals? Preliminary studies by ATR-FTIR spectroscopy and chemometrics. *Spectrochimica Acta Part: Molecular and Biomolecular Spectroscopy* **2017**, *171*, 280-286. Doi: <https://doi.org/10.1016/j.saa.2016.08.003>.
6. Edwards H.C.; Rossi M.; Corpe C.P.; Butterworth P.J. The role of sugars and sweeteners in food, diet and health: Alternatives for the future. *Trends in Food Science & Technology* **2016**, *56*, 158-166. Doi: 10.1016/j.tifs.2016.07.008.
7. Salman M. T.; Olaky L.A.; Alagbonsi I. A.; Yewopo A.O. Spermatotoxic effects of galactose and possible mechanisms of action. *Middle East Fertility Society Journal* **2016**,

- 21, 82-90. Doi: <https://doi.org/10.1016/j.mefs.2015.09.004>.
8. Lustig R.H. Fructose: Metabolic, Hedonic and Societal Parallels with Etanol. *Journal of the American Dietetic Association* **2010**, *110*, 1307-1321. Doi: <https://doi.org/10.1016/j.jada.2010.06.008>.
  9. Ackroff K.; Sclafani A. Rats' preferences for high fructose corn syrup vs. sucrose and sugar mixtures. *Physiology & Behavior* **2011**, *102*, 548-552. Doi: <https://doi.org/10.1016/j.physbeh.2011.01.004>.
  10. Avena M.; Rada P.; Hoebl B. G. Evidence for sugar addiction: Behavioral and neurochemical effects of intermittent, excessive sugar intake. *Neuroscience & Biobehavioral Reviews* **2008**, *32*, 20-39. Doi: <https://doi.org/10.1016/j.neubiorev.2007.04.019>.
  11. Havel P.J.; Keim N.L. FRUCTOSE. *Encyclopedia of Human Nutrition (Second Edition)*. **2005**, 351-356. Doi: <https://doi.org/10.1016/B0-12-226694-3/00141-1>.
  12. Giri B.; Dey S.; Das T.; Sarkar M.; Banerjee J.; Dash K.S. Chronic hyperglycemia mediated physiological alteration and metabolic distortion leads to organ dysfunction, infection, cancer progression and other pathophysiological consequences: An update on glucose toxicity. *Biomedicine & Pharmacotherapy* **2018**, *107*, 306-328. Doi: <https://doi.org/10.1016/j.biopha.2018.07.157>.
  13. Quincozes-Santos A.; Bobemin L. D.; Assis A. M.; Goncalves C.A.; Souza D.O. Fluctuations in glucose levels induce glial toxicity with glutamatergic, oxidative and inflammatory implications. *Biochimica et Biophysica Acta (BBA) - Molecular Basis of Disease* **2017**, *1863*, 1-14. Doi: <https://doi.org/10.1016/j.bbadis.2016.09.013>.
  14. Hanover M. L. Functionality of Corn-Derived Sweeteners in Formulated Foods. *Chemistry of Foods and Beverages: Recent Developments* **1982**, 211-233. Doi: <https://doi.org/10.1016/B978-0-12-169080-9.50015-7>.
  15. Ochoa M.; Malbert C.H.; Lalles J.P.; Bobillier E.; Val-Laillet D. Effects of chronic intake of starch-, glucose- and fructose-containing diets on eating behaviour in adult minipigs. *Applied Animal Behaviour Science* **2014**, *157*, 61-71. Doi: <https://doi.org/10.1016/j.applanim.2014.05.010>.
  16. Matrocola R.; Ferrocino I.; Liberto E.; Chiazza F.; Cento A.S.; Collotaa D.; Querio G.; Nigro D.; Bitonto V.; Cutrin J.C.; Rantsiou K.; Durante M.; Masini E.; Argano M.; Cordero C.; Cocolin L.; Collino M. Fructose liquid and solid formulations differently affect gut integrity, microbiota composition and related liver toxicity: a comparative in vivo study. *The Journal of Nutritional Biochemistry* **2018**, *55*, 185-199. Doi: <https://doi.org/10.1016/j.jnutbio.2018.02.003>.
  17. Liu G.; Hale G.E.; Haugles C.L. Galactose metabolism and ovarian toxicity. *Reproductive Toxicology* **2000**, *14*, 377-384. Doi: [https://doi.org/10.1016/S0890-6238\(00\)00096-4](https://doi.org/10.1016/S0890-6238(00)00096-4).
  18. Saphiro F.; Mahagna M.; NIR I. Stunting Syndrome in Broilers: Effect of Glucose or Maltose Supplementation on Digestive Organs, Intestinal Disaccharidases and Some Blood Metabolites. *The Hebrew University of Jerusalem, Faculty of Agriculture, Dept. of Animal Science, P.O. Box 12, Rehovot 76100, Israel* **1996**, *76*, 369-380.
  19. Clouard C.; Chataigner M.; Meunier-Salaun M-C.; Val Laillet D. Flavour preference acquired via a beverage-induced conditioning and its transposition to solid food: Sucrose but not maltodextrin or saccharin induced significant flavour preferences in pigs. *Applied Animal Behaviour Science* **2012**, *136*, 26-36. Doi: <https://doi.org/10.1016/j.applanim.2011.11.007>.
  20. Guidance document on the validation of (Quantitative)Structure-Activity Relationships [(Q)SAR] Models. OECD 69, **2007**.

21. European Food Safety Authority, Modern methodologies and tools for human hazard assessment of chemicals, *EFSA Journal* **2014**, *12*, 3638.
22. Craciun D.; Modra D.; Isvoran A; ADME-Tox profiles of some food additives and pesticides. *AIP Conference Proceedings* **2015**. Doi: <https://doi.org/10.1063/1.4937259>.
23. Isvoran A.; Ciorsac A.; Ostafe V. ADME-Tox profiling of some low molecular weight water soluble chitosan derivatives. *ADMET&DMPK* **2017**, *5*, 192-200 . Doi: <http://dx.doi.org/10.5599/admet.5.3.423>.
24. Roman M.; Roman D.L.; Ostafe V.; Ciorsac A.. Computational assessment of pharmacokinetics and biological effects of some anabolic and androgenic steroids. *Pharmaceutical Research* **2018**, *35*. Doi: 10.1007/s11095-018-2353-1.
25. Roman M. ; Roman D.L. ; Ostafe V. ; Isvoran A. Computational Assessment of Biological Effects of Methyl-,Ethyl-, Propyl- and Butyl-Parabens. *Journal of Bioinformatics, Genomics, Proteomics* **2018**, *3*, Doi: <https://www.jscimedcentral.com/Bioinformatics/bioinformatics-3-1029.pdf>.
26. Alves V.M.; Muratov E.N.; Zakharov A.; Muratov N.N.; Andrade C.H.; Tropsha A. Chemical toxicity prediction for major classes of industrial chemicals:Is it possible to develop universal models covering cosmetics, drugs, and pesticides?. *Food and Chemical Toxicology* **2018**, *112*, 526-534.Doi: <https://www.ncbi.nlm.nih.gov/pmc/articles/PMC5638676/>.
27. Gridan M.I.; Ciorsac A.; Isvoran A. Prediction of ADME-Tox properties and toxicological endpoints of triazole fungicides used for cereals protection, *ADMET & DMPK* **2019**, *7*, 161-173. Doi: <http://dx.doi.org/10.5599/admet.668>.
28. Roman D.L.; Roman M.; Som C.; Schmutz M.; Hernandez E.; Wick P., Casalini T, Perale G, Ostafe V., Isvoran A., Computational assessment of the pharmacological profiles of degradation products of chitosan. *Frontiers in Bioengineering and Biotechnology* **2019**, *7*. Doi: <https://doi.org/10.3389/fbioe.2019.00214>.
29. Craciun D.; Dascalu D.; Isvoran A. Computational assessment of the adme-tox profiles and harmful effects of the most common used phthalates on the human health. *STUDIA UNIVERSITATIS BABES-BOLYAI CHEMIA* **2019**, *64*, 71-92.
30. Daina A.; Michielin O.; Zoete V. SwissADME: a free web tool to evaluate pharmacokinetics, drug-likeness and medicinal chemistry friendliness of small molecules. *Sci. Rep.* **2017**, *7*. Doi: 10.1038/srep42717.
31. Poroikov V.; Filimonov D., Lagunin A.; Glorizova T.; Zakharov A. PASS: Identification of probable targets and mechanisms of toxicity. *SAR & QSAR in Environmental Research* **2007**, *18*, 101-110. Doi: 10.1080/10629360601054031.
32. Vilar S.; Costanzi S. Predicting the biological activities through QSAR analysis and docking-based scoring. *Methods Mol Biol.* **2012**, *914*, 271–284. Doi:10.1007/978-1-62703-023-6\_16.
33. Lipinski C.A.; Lombardo F.; Dominy B.W.; Feeney P.J. Experimental and computational approaches to estimate solubility and permeability in drug discovery and development settings. *Adv. Drug Deliv* **2001**, *46*, 1–3. Doi:10.1016/S0169-409X(00)00129-0.
34. Irwin J.J.; Sterling T.; Mysinger M.M.; Bolstad E.S.; Coleman R. G. ZINC: A Free Tool to Discover Chemistry for Biology. *J. Chem. Inf. Model* **2012**. Doi: 10.1021/ci3001277.
35. Poroikov V.; Filimonov D.; Lagunin A.; Glorizova T.; Zakharov A. PASS: Identification of probable targets and mechanisms of toxicity. *SAR & QSAR in Environmental Research* **2007**, *18*, 101-110. Doi: 10.1080/10629360601054031.

- 
36. Atkinson, F.; Cole S.; Green C.; Van de Waterbeemd H. Lipophilicity and other parameters affecting brain penetration. *Cent. Nerv. Syst. Agents. Med. Chem.* **2002**, *2*, 229–240.
  37. Hitchcock, S.A. Structural modifications that alter the P-glycoprotein efflux properties of compounds. *J. Med. Chem.* **2012**, *55*, 4877. Doi: 10.1021/jm201136z.
  38. Tappy L. Toxic' effects of sugar: should we be afraid of fructose? *BMC Biology* **2012**, *10*:42. Doi: 10.1186/1741-7007-10-42.
  39. Bomback A.S.; Derebail V. K.; Shoham D. A.; Anderson C.A.; Steffen L. M.; Rosamond W. D.; Kshirsagar A. V. Sugar-sweetened soda consumption, hyperuricemia, and kidney disease. *Kidney Int.* **2010**, *77*, 609–616. doi:10.1038/ki.2009.500.
  40. Zang D.J.; Spreen A.N.; LaValle J.B. Smart Medicine for Healthier Living. *Garden City Park, New York, SUA*, **1999**.
  41. Mohammad M.A. ; Sunehag A.L.; Rodriguez L.A.; Haymond M.W. Galactose promotes fat mobilization in obese lactating and nonlactating women. *Am J Clin Nutr.* **2011**, *93*, (2):374–381. doi:10.3945/ajcn.110.005785.

Article

## OBTAINING EXTRACTS FROM MORNING GLORY. PHARMACOTOXICOLOGY

*Iacob Gabriel-Constantin<sup>1</sup>, Duda Seiman Corina<sup>1\*</sup>, Adina Negrea<sup>2</sup>,  
Dan Marculescu<sup>3</sup>*

1 Department of Biology-Chemistry, Faculty of Chemistry, Biology, Geography, West University of Timișoara, 16A Pestalozzi Street, 300115, Timișoara, Romania

2 Universitatea Politehnica Timisoara, 2 Victoriei Square, 300006, Timișoara, Romania

3 Spitalul Clinic Municipal Deva,

### ABSTRACT

In the early 1930s, Japanese researchers made the first genetic map of plants using flowers with variations in color from the genus *Ipomoea*. Recent studies have placed eyebrows as a model for understanding the genes involved in flower color. Current work with *Ipomoea* species raises a series of evolutionary questions that apply to many biological organisms and processes. There is a great appreciation of this kind of flowers because it is very versatile in terms of studies on their systems.

**Keywords:** morning glory, bio-active compounds, toxicity

### 1. INTRODUCTION

The genus *Ipomoea* along with its species, the most famous of which are the cornflowers, raised many questions over time about its evolution. The genre presents a wide diversity in environmental tolerance, flower color, form of growth, and research has been very intense over the past 80 years.

The term "buckwheat" refers to the fact that these plants have an impressive start, but which fades quickly, supported by the fact that the flowers open early in the morning, but wither until the afternoon. This aggressive feature does not, however, affect the production of flowers or seeds, so the plant is easy to grow in both greenhouses and fields. All these qualities have led to the use of the *Ipomoea* genus in organic genetics. Current studies on zorls began in 1970, but continue today, and their commemoration in literature is about 80 years. The current work with the owls and the rest of the *Ipomoea* species raises many questions about evolution, questions about many organisms and biological processes. These questions are diverse, from the evolution of the reproductive system, to the interaction with herbivores and parasitic plants (Baucom et al. 2011; Wang et al. 2017; Kinori et al. 2018).

## 1.2 Botanical description of morning glory

The *Convolvulaceae* family, of which the morning glory belong, has many representatives, from those with very tall vines and woody linden trees in tropical forests to perennial plants. Morning glory are appreciated and cultivated by humans for the beautiful trumpet flowers and their very attractive leaves.

The species of corolla are the most common in Asia and tropical America, but because they spread so easily they are also found in temperate and subtropical areas. Vine and clover grow at a very high speed and usually begin at the edge of the forests or near the lakes where the trees fell and the sun penetrates vigorously. Having a lot of competition for light and space, they grow very fast, even to the top of the trees, to facilitate photosynthesis, special adaptation of some species.

Although there are dozens of different genus types, with slightly different floral features, leaves and fruits are also slightly different, all have the same thing in common: their flowers are funnel-shaped and colors like purple, blue, white, yellow or red. We have forgotten to mention a very important representative, *Ipomoea aquatica* or water spaniel, which originated in China. It is often cultivated in China, India, Malaysia, Central America, the West Indies and Brazil, and is a green vegetable. Some Asian restaurants serve customers and are also found on Asian markets in Southern California.

Being a tasty plant was naturalized in Australia and some countries in Africa, South America and the Pacific. It can replace native plants, thus destroying habitats of wild fish and animals.

Perhaps the most famous representative of the *Convolvulaceae* family is *Ipomoea batatas* (sweet potato). Probably brought by Christopher Columbus from America is highly appreciated for its sweet-tasting root.

The Mexican horns *Ipomoea violacea* and *Turbina corymbosa* were taken by the Aztec priests and drunk to communicate with their gods.

Due to the extremely fine line between the lethal effect and the desired effect, they were only used by the experienced ones. The effect is given by the ergoline alkaloid. Before it was discovered, the ergin was known only from ergot (*Claviceps purpurea*), a rust fungus that infects the beans. In the Middle Ages, thousands of people in Europe were affected by ergotism, a malady characterized by madness, gangrene and seizures. Maladia started because they ate infected bread with *Claviceps purpurea*. (Petruzzello 2019)

## 1.3 Bio-active compounds from morning glory

Until now, in *Ipomoea purpurea* was identified 25 volatile compounds, of which 17 had retention times for GC-MS methods. No benzenoid or volatile phenpropanoid have been identified in the studies, although some *Ipomoea* species such as *Ipomoea langifolia* and *Ipomoea Alba* emit aromatic compounds such as methylsilicate and methylbenzionate.

Subsequently, extracts from leaves and dried seeds were made from *Ipomoea Alba*. These extracts have been found to exhibit a complex of oligosaccharides, monohydroxy and dihydroxy C-14 and C-16 which are some fatty acids which are zorrel-specific secondary metabolites.

Another representative of the *Ipomoeae* genus that causes many deaths in Brazil is *Ipomoea asarifolia*. Previous studies show that lectin may be involved in toxic effects. To reinforce this hypothesis a lectin fraction of *Ipomoea asarifolia* was isolated and its effects evaluated. The leaves were removed from the plant, kept in a room with a relative humidity of approximately 100% at 25 +/- C for 72 hours in the dark.

The in vivo toxicity of the leaves was tested by intraocular injection of the mice. They showed uncontrollable, clumsy movements, but without death. Toxin reduces the ability of muscles to contract up to 50%, which affects the inhibition of neurotransmitters.

It was injected into the kidney of the mice, with no visible effects on vascular resistance and pressure, but with an increase in glomerular filtration. In addition, the percentage of tubular transport, and decreased. After a histological examination of the kidneys, minor alterations were reported, which proved the toxic nature of lectin. (Rice & Genest, 1965)

#### **1.4 Aspects of pharmacology and pharmacotoxicology of bio-active compounds from morning glory**

The potential for sharing biochemical pathways between pigments and volatile substances has received particular attention. There are at least two independent sources of biosynthetic connections among these floral characters. One of the greatest importance in medicine is *Convolvulus pluricaulis*, an important representative of the Convolvulaceae family, recognized for its versatility and treatments.

It is a good cure against high blood pressure, vomiting, ulcer, epilepsy and neurodegenerative diseases. It is also used to lower cholesterol and improve memory. In traditional practices it is even used as a memory supplement. Reduces mental tension and acts as an anesthetic, "tranquilizer". We're talking about a tranquilizing effect because recent pharmaceutical studies suggest that. (Kumar 2007)

Clinical studies of *Convolvulus pluricaulis* show that it has beneficial effects on patients with anxiety. Induce a sense of calm and tranquility, tranquil sleep, relieving stress and eliminating mental fatigue. Phytochemical screening performed on the ethanol extract from *Convolvulus pluricaulis* showed the presence of phytoconstituents such as alkaloids, glycosides, sterol, mucilages, carbohydrates and protein. (Gupta et al. 2005)

The various pharmacological and structural properties show that alkaloids and steroids have been found in compounds that can explain the traditional therapeutic effects. Some preparations have been subjected to clinical tests, the preparations being administered as syrup and tablets. (Agarwa et al. 2014)

#### **1.5 Suicide cases with morning glory**

There is a famous suicide case with seeds containing LSA. Two men aged 29 (deceased) and 25 (witness who survived). The seeds were soaked in water for about 2.5-3 hours and then ingested by the subjects. The witness ingested six seeds, and he could not remember how much he had consumed. Shortly afterwards, both subjects consumed cannabis (Ahimsa-Mueller et al. 2007)

Approximately 40 minutes after ingestion, the witness had feelings of well-being, but also the sense that time passed very quickly. Approximately 3 hours after ingestion, the 29-year-old subject (deceased) showed very intense agitation and jumped off the window falling on 4 floors. (Schultes & Hofmann 1980)

At autopsy, the toxicological analysis was done 13 hours after ingestion. The report specified cranial contusions, multiple fractures of the pelvis and ribs, lacerations of the right lung, cardiac contusion, rupture of the artery and arteriosclerosis. Blood and urine of the witness were taken 9 hours after ingestion (Klinke et al. 2010)

The more LSA-containing seeds are found in stores and marketed online. Some buy them for legitimate purposes and others strictly for hallucinogenic effects. LSA is classified as a precursor to LSD. (Cohen 1964)

## 2. METHOD/MODEL

For the extract, dry material was used, namely *Ipomoea purpurea* seeds and *Ipomoea tricolor* seeds. The extraction method used was cold maceration, carried out at room temperature (17-24 °C). As solvents I used water for *Ipomoea purpurea*, namely alcohol for *Ipomoea tricolor*. The powder of *Ipomoea purpurea* weighed 1.8222 mg, and the *Ipomoea tricolor* powder had the weight of 2.0611 mg.

After crushing, the powder was placed in the solvent, each in its solvent, and then filtered under vacuum. The preparations were for a period of 24 hours, after which filtration was performed. The obtained extract was processed by IR and UV spectroscopic methods for the identification of bioactive compounds in the gills.

It has been preferred to use cold maceration since this avoids the precipitation of the bioactive substances obtained from the extract. If we had used methods such as infusion or decoction, there was a good chance that substances would precipitate. As this process is carried out at room temperature, it can only be an advantage for making the preparation.

The extracts were made in 98% ethyl alcohol. The only disadvantage of cold maceration is that sometimes if it is made with a solvent other than water or alcohol, such as oil, wine, vinegar, etc., the separation time is prolonged a lot and can even reach a few weeks.

### 2.1. Theoretical Method/Model

Heat precipitates extracted bioactive substances, which is why cold extraction is preferred in exchange for decoction or infusion. It has many advantages in terms of being at room temperature and, besides, it is the simplest way to extract. It also implies the presence of a solvent, which is usually water or a mixture of water and alcohol. The plant product to be macerated is kept in constant contact with the chosen solvent and has to be agitated at different time intervals. The maceration time is variable; at the end of the process the extract is separated.

### 2.2. Experimental Method/Model

Cold maceration is performed at room temperature (C). The product and solvent remain in contact for a determined period, for example if the solvent is water for 8-12 hours. If the maceration had occurred warm it would have been done at a temperature of C. Separation of the product can be done by filtration or decantation. Exit and macerate which is made in other solutions, eg vinegar, oil, wine. If the maceration is done with one of these solutions, the separation is much longer, in some cases reaching a few weeks.

If we have to relate to the process, we have simple, double or repeated maceration. The simple one was not very efficient because it had low yields, so it was repeated and doubled maceration. In this case contact with solvent is unique. The double maceration is somewhat more complex; the extracted product is mixed with the solvent in a ratio of 1/2 to 2/3. The resulting residue is pressed and the liquid is separated. A new amount of extractive solution resulting from the contact between the pressed residue and the solvent residue will be obtained.

Once the liquids are joined and run for 24 hours, they will be filtered. Repeated maceration is the most complex. The product is treated with a variety of solvents, all after being cut, and then stored in closed containers all the time. After pressing the plant product, it is in contact with

what remains of the solvent until the total volume of the extractive liquid is completely exhausted.

After that the portions to be obtained are mixed. This method avoids the scattering of the active principles that can remain in the maceration residue, as happens for simple maceration. Macerata should be kept in a refrigerator, preferably in closed glass pots.

The maximum storage life is 2-3 days. If the retention period is prolonged, the development of microorganisms is likely. Besides this there is the risk of degrading the active principles in an irrecoverable way (Paun et al. 2011)

### 3. IR & UV ASSESMENT

IR spectroscopy or infrared spectroscopy is a technique that involves tracking interactions between matter and infrared radiation. Assume the absorption of wavelengths in the infrared range. However, the absorption is carried out in accordance with the characteristics of the chemical structures.

IR spectroscopy utilizes wavelengths ranging between 750nm-100 $\mu$ m. Frequencies that match the transition energy of a link or the vibration of a group within a molecule are called resonant frequencies. An n-atom molecule normally has 3n-6 normal ways in which it can vibrate. In the case of 3n-5 we have a linear molecule, that is, the rhorthole around its molecular axis can not be detected.

Generally, radiation studies the photons strictly, but if we relate to spectroscopy, we can see that it also deals with electrons, phonons, or protons. If it also refers to these aspects, it automatically refers to the state of aggregation of the product that will interact with the radiation emitted. (Stef 2017)

UV spectroscopy analyzes quantitatively and qualitatively everything related to UV absorption spectra (UV-visible). This is only the case if the substances are in a solid or liquid state and only if we refer to organic and inorganic substances. One thing to note in UV spectroscopy is that the focus falls on quantitative analysis rather than on qualitative analysis. This is due to the fact that not all spectra of substances have clear maxima. The Lambert-Beer Law established a correlation between absorbance A, length of radiation pathway and sample concentration C. (Andu Jothi & Geetha 2017)

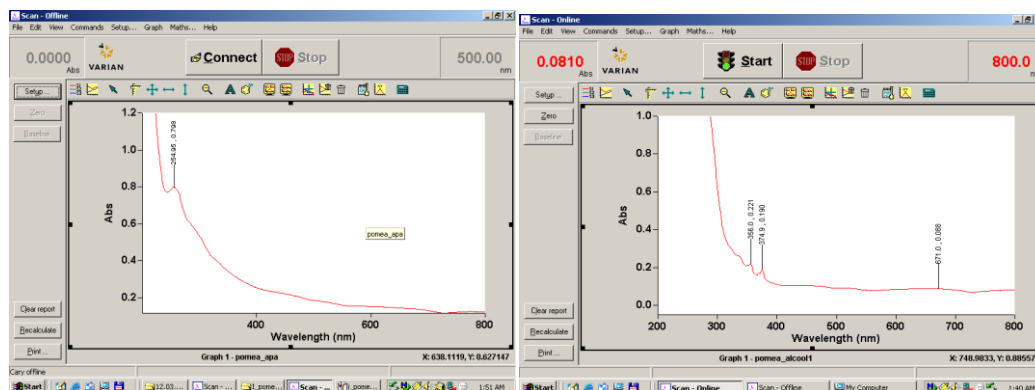
#### 3.1. Results

The results obtained are represented (see Figures 1 and 2) and analyzed. The specimen was used to identify the bioactive compounds present in both *Ipomoea purpurea* and *Ipomoea tricolor*.

Within the IR spectrum for species of the genus *Ipomoea*, the compounds and lengths of them may be:

- the wavelength 3405.75 shows a 44% transmittance corresponding to the prolonged N-H leg of pyrolites
- at wavelength 2920.56, a 12% transmittance corresponding to the elongated C-H bond in the alkanes
- at the wavelength 2850.95, a 20% transmittance of the elongated C-H bond from the alkanes
- the wavelength of 1647.72 shows an 18% transmittance of the elongated N-H bond of the secondary amines
- at the wavelength of 1544.87 there is a 28% transmittance corresponding to the elongated bond from the nitro tertiary compounds
- the wavelength of 1384.45 shows a 25% transmittance corresponding to the alkane deformed bond

- at the wavelength 1320.12 there is a 36% transmittance corresponding to the elongated S = O bond of the sulfur compounds
- the wavelength of 1255.05 shows a 10% transmittance corresponding to the elongated O-R bond from aliphatic esters (CH<sub>3</sub>COOR)
- at the wavelength 1155.75 there is a 32% transmittance corresponding to the S = O elongation from the sulfones
- the wavelength 1051.63 shows a 22% transmittance corresponding to the S = O elongation from the sulfonic acid
- at a wavelength of 919.94, a 68% transmittance of the deformed C-H bond from mono-substituted alkanes
- at the wavelength of 618.99 there is a 40% transmittance corresponding to the elongated C-Cl bond of the halides
- At the wavelength of 532.06, a 42% transmittance of the elongated C-Br bond from the bromides
- the wavelength 445.08 shows a 55% transmittance of the iodine elongated C-I bond (Andu Jothi & Geetha.2017)

Fig 1. *Ipomoea purpurea* in waterFig2. *Ipomoea tricolor* in alcohol

In the UV spectrum, the results show that:

- for *Ipomoea purpurea*, at a wavelength of 254.95, 0.798, there is a 0.9 nm absorbance corresponding to the Cy2C4G component
- for *Ipomoea tricolor*, at a wavelength of 356.0, 0.221 there is a 0.3 nm absorbance corresponding to the Pg3C5G component
- for *Ipomoea tricolor*, at a wavelength of 374.9, 0.190, there is a 0.25 nm absorbance corresponding to the Pg3C4G component
- for *Ipomoea tricolor*, at a wavelength of 671.0, 0.088 there is an absorbance of 0.2 nm corresponding to the Cy3C5G component (Chandran et al. 2012)

### 3.2. Discussion

There have been reports of mental degradation after harvesting of the seabuckthorn, publicized cases for population prevention. Mental degradation has often led to suicide cases from subjects who have ingested semen seeds. Studies have shown that plants have developed methods of insect defense, and insects require a natural selection of plants. Furthermore, insecticide treatments have shown that plants have developed more seeds in the absence of insects, and insecticide treatment has not produced genetic or evolutionary variations. For this purpose, it has been found that using empirical data and theories, the understanding of evolution can be made by understanding the tolerance and resistance of plants of this genre.

### 4. CONCLUSIONS

Morning glory is an extremely diverse family, being the most known members of the genus *Ipomoea*, highly appreciated in all corners of the world for their beauty.

With a very fast growth rate and pleasant appearance are grown on a large scale, having an important economic role. Perhaps the most important role of alkaloids in their seeds, being much studied for their properties.

It has a very large variety, *Ipomoea tricolor* and *Ipomoea purpurea* (both ornamental), *Ipomoea violacea* (used in religious ceremonies), *Ipomoea Alba* (used in the rubber industry), *Ipomoea leptophylla* and *Ipomoea arborescens* (present in the form of trees or shrubs) and even *Ipomoea batatas* (sweet potato).

The most important bioactive compounds in the eyebrows are alkaloids, which give the seeds different properties, from reducing blood pressure, stopping vomiting or neurodegenerative diseases to effects and conditions similar to LSD consumption.

Morning glory have LSA, an LSD-like alkaloid, which leads to the testing of seeds in different forms by many people.

The most notorious case of death in corn consumption occurred in the US, where two men of 24 and 25 years of age consumed seed water, and after a few hours the 29-year-old died.

In the present work I made cold extracts in ethyl alcohol 98% of the seeds of the corn.

The obtained extracts were by IR and UV spectroscopic methods. The following types of bioactive compounds have been identified: alkaloids in particular

In terms of toxicity, doses higher than 200 mg / kg are fatal.

Due to the compounds present in *Ipomoea purpurea* and *Ipomoea tricolor*, but also in the rest of *Ipomoea* representations, they are of great pharmacological and pharmacotoxicological interest.

### REFERENCES

Agarwa, P., Sharma, B., Fatima, A & Jain, S.K., An update on Ayurvedic herb *Convolvulus pluricaulis* Choisy, *Asian Pacific Journal of Tropical Biomedicine*, 245-252, 2014

Ahimsa-Mueller M.A., Markert A., Helwing S., Knoop V., Steiner U., Drewke C., Leinstre E., Clavicipitaceous fungi associated with ergo line alkaloid-containing, *Convolvulaceae*, *J. Nat. Proud.* 70(2007) 1955-1960

Andu Jothi B., Geetha B., GC-MS and FT-IR analysis of bioactive compounds on methanol extract of *Ipomoea aquatica*, *International Journal of Fisheries and Aquatic Research*, Volume 2, Issue 3, pp 12-16, May 2017

Baucom R.S., Chang S-M, Kniskern J.M., Rausher M.D., Stinchcombe J.R., Morning Glory as a powerful model in ecological genomics: tracing adaptation through both natural and artificial selection, *Heredity* 107, pp. 377-385, 2011

Chandran A., Mary S., Varghese H.T., Panicker C.Y., Manojkumar T.K., Van Alsenoy C., Rajendran G., Vibrational Spectroscopic Study of (E)-4-(Benzylideneamino)-N-Carbamimidoyl Benzenesulfonamide, International cholarly Research Network, *ISRN Analytical Chemistry*, Volume 2012, Article ID 397026, 11 pages, 2012

Cohen, S. Suicide following morning glory seed ingestion, *American Journal of Psychiatry*, 120(10), 1024-1025, 1964

Gupta A.K., Tandon N, Sharma M. *Quality standards of Indian medicinal plants*. New Delhi: Indian Council of Medical Research, 2005

Kinori M. Smiley N. P., & Zeid, J. L., Morning glory disc anomaly and ipsilateral sporadic optic pathway glioma, *American Journal of Ophthalmology Case Reports*, 10, 16-17, 2018

Klinke H.B., Muller I.B., Steffenrud S., Dahl-Sorensen R., Two cases of lysergamide intoxication by ingestion of seeds from Hawaiian Baby Woodrose, *Forensic Science International*, Volume 197, Issues 1-3, pp. e1-e5, 15 April 2010

Kumar DC. Pharmacognosy can help minimize accidental misuse of herbal medicine, *Curr Sci*, 1356-1358, 2007

Păun G., Gheorghe O., Diaconu M., *Advanced Processing of Medicinal Plants* (Originally in Romanian as: Curs procesare avansată a plantelor medicinale) pp. 8-12, 2011

Petruzzello M., Morning Glory, *Encyclopedia Britannica*, 8 march 2019.

Rice W.B, Genest K., Acute Toxicity of Extracts of Morning-glory Seeds in Mice, *Nature* 207, 302-303, 1965

Schultes R.E., Hofmann A., *The Botany and Chemistry of Hallucinogens*, Charles C. Thomas, Springfield, IL, 1980

Ștef M., *Spectroscopy and lasers, Course notes* (Originally in Romanian as: Spectroscopie și laseri, Notițe de curs), West University of Timisoara, 14 December 2017

Wang S., Hang X., Zhu X., Han H., Zhang G., & Liao W., 1D morning glory-like calixarene-based coordination polymers as a support for Au/Ag nanoparticles, *Polyhedron*, 130, 75080, 2017

Article

# CHARACTERIZATION OF BENZENE AND CORONENE MOLECULES AS SUBSYSTEMS OF A GRAPHENE NANORIBBON IN DIFFERENT BONDING STATES

*Marina Alexandra Tudoran<sup>1</sup>, Mihai V. Putz<sup>1,2\*</sup>*

<sup>1</sup>National Institute for Research and Development in Electrochemistry and Condensed Matter, Laboratory of Renewable Energies – Scientific, Str. Prof. Paunescu-Podeanu 144, Timisoara 300569, Romania

<sup>2</sup>West University of Timisoara, Faculty of Chemistry-Biology-Geography, Biology – Chemistry Department, Laboratory of Structural and Computational Physical-Chemistry for Nanosciences and QSAR, Str. Pestalozzi 16A, Timisoara 300115, Romania

## ABSTRACT

Following the transdisciplinarity trend in science, this study was design to presents a way in which mathematical functions can be used in molecular characterization. Thus, the selected working system is a graphene nanoribbon consisting in 25 fused benzene rings, divided in two sub-systems i.e. unit cell and hypercell. For the two selected sub-systems, first was determined their physico-chemical parameters, than the obtained values were computed using the Heaviside based Gradient function formula, leading to a new set of parameters which can also offers new information about the working system.

**Keywords:** graphene nanoribbon, benzene, atomic gradient, wave equation, Heaviside (Gradient) function.

## 1. INTRODUCTION

Graphene has attracted a lot of attention in the last years due to the fact that exhibit extraordinary physical and mechanical properties, i.e. is considered stronger than steel, very flexible and light, having at the same time high thermal and electronic conductivities. In literature, graphene is known as a carbon allotrope with the shape of a bi-dimensional crystal with  $sp^2$  orbital hybridization and 0.34 nm thicknesses. In graphene, each carbon atom is

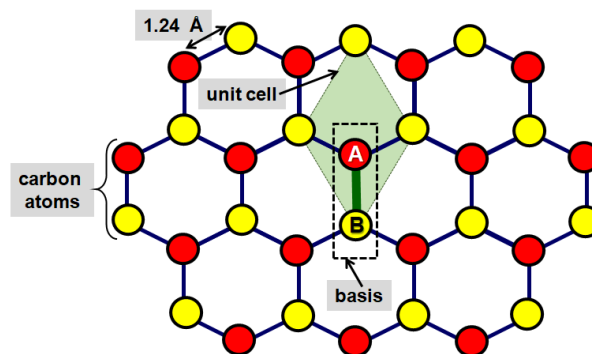
---

\* Correspondent author: mihai.putz@e-uvt.ro

bonded with other three carbon atoms, resulting in a very stable hexagonal lattice (in order to form a chemical bond with graphene, the  $sp^2$  bond must be converted into a  $sp^3$  bond). A graphene sheet can be "cut" into thin nanoscale ribbons, thus being created structures with a finite number of benzene rings called graphene ribbons (GNR). Besides, graphene is also the basic structure for fullerenes, carbon nanotubes and graphite [1-5].

As the sixth element in the periodic table, carbon has six protons in the nucleus and six electrons, the latter filling the lowest three orbitals in the arrangement  $[1s]^2[2s]^2[2p]^2$ ; type  $|s\rangle$  orbitals are spherical and symmetrical,  $|p\rangle$  type orbitals are elongated along a linear axis. If the carbon atoms approach each other, the two electrons from the  $[1s]^2$  orbitals do not participate on the bond formation (they remain close to the nucleus), the ones involved in the chemical bonds being the outermost orbitals. Thus, different form of carbon can be constructed due to the fact that there are different ways in which the four electrons in the outer orbitals  $[2s]^2[2p]^2$  can be divided between atoms.

**Figure 1:** Grafene lattice with basic structural units; [4]



The  $sp^3$  bond is tetrahedral (3D) and is formed when a carbon atom equally share its four electrons with four nearest carbon atoms (e.g. the crystal structure of the diamond). Electrons in carbon atoms can also combine with hydrogen atoms [4] and form  $sp^2$  or  $sp$  bonds (e.g. 2D planar molecules - benzene, or long one-dimensional chains - conductive polymers).

In his work, Debdeep [4] presents the crystalline structure of graphene considering two nearest-neighbor carbon atoms as the smallest unit which can be translated over the entire 2D space of the graphene plane (Figure 1). The author states that the two carbon atoms (denoted by A and B) are not identical due to the fact that the electronic wave function associated with them can break the "mechanical" symmetry. The  $sp^2$  bond, characteristic of graphene, is denoted by  $|sp^2\rangle = a|s\rangle + b|px\rangle + c|py\rangle$  with  $a, b, c$  - constants, and is formed when a carbon atom shares electrons with three of its nearest neighbors, leaving one electron free for each carbon atom [4]. The electrons energies composing the  $sp^2$  bonds constitute the so-called  $\sigma$  bands, which gives graphene its vibrational and structural properties (e.g. Young's modulus, thermal conductivity, etc.), being also responsible for its perfectly flat nature. The electrons which do not participate in the chemical bond formation come from the  $|p_z\rangle$  orbitals and can move between the nearest neighboring carbon atoms with a hoop energy of  $\gamma_0 \sim 3.0 eV$ ,

having delocalized wave functions [4]. Thus, the allowed energies of these electrons constitute the so called  $\pi$  bands. The delocalized electrons are responsible for the exceptional electrical conductivity of graphene, their allowed energies depending on their wavelength, following the rules of quantum mechanics. Moving forward, one will consider the de-Broglie relation, which states that the wavelength is inversely proportional to the momentum. Thus, the momentum is expressed by  $\hbar k$ , with  $\hbar$  - the Planck's constant, and  $k = 2\pi / \lambda$  with  $\lambda$  - the wavelength. If one will consider the basis of two atoms, the wavefunctions of graphene electrons can be represented as "spinors", i.e. two components matrices of the form  $\frac{\exp[ik \cdot r]}{\sqrt{2}} \begin{pmatrix} 1 \\ \exp[i\theta] \end{pmatrix}$  with  $k = xk_x + yk_y$  and  $\tan \theta = k_y / k_x$  [4].

On the other hand, Green's function is widely used in electrodynamics and quantum field theory [6], especially for problems where the relevant differential operators are often difficult or impossible to solve exactly (but can be solved in a perturbative way using Green's functions). There are many definitions for Green's function known in literature, depending on its representation domain and its application [7].

In his work, Rastegin [8] derive the Green's function of the wave equation by considering that the non-homogeneous wave equation for a field described by a function of the scalar potential  $\phi(r,t)$  can be written as following:

$$\nabla^2 \phi - \frac{1}{c^2} \frac{\partial^2 \phi}{\partial t^2} = Q(r,t) \quad (1)$$

with  $Q(r,t)$  - the function describing the source of action, with the physical meaning determined by the considered processes nature; the model is linear (i.e. Eq. (1)), and as a result, this equation allows overlapping solutions.

Thus, for a source  $Q$  represented as the sum of two other sources, e.g.  $Q_1$  and  $Q_2$ , with several solutions  $\phi_1$  and  $\phi_2$ , known for each of them separately, a solution of the previous equation can be of the form:

$$\phi(r,t) = \phi_1(r,t) + \phi_2(r,t) \quad (2)$$

Based on these considerations, the author [8] considers the Green function as a viable method for solving inhomogeneous linear models; in this case, the given source is represented in the form of some "elementary" sources superpositions with known solutions.

More precisely, the inhomogeneous equation is considered as follow:

$$\nabla^2 \psi = \rho(r) \quad (3)$$

with  $\psi(r)$  - an abstract potential, and  $\rho(r)$  - describes the sources distribution. Eq. (3) can be solved using the integral:

$$\psi(r) = \int G(r,R) \rho(R) dV_R \quad (4)$$

whit  $G(r,R)$  as the Green's function with standard expression  $G(r,R) = -\frac{1}{4\pi|r-R|}$  which

depends only on  $|r-R|$ .

Starting from these considerate, the author [8] proceeds in his study by deriving the Green function for the wave equation, starting from considering a material point which varies in time, located at the coordinate origin, of the form:

$$Q(r,t) = \delta(r)q(t) \quad (5)$$

as the source for the inhomogeneous wave equation Eq. (1).

Thus, Eq. (1) with the source as Eq. (5) constitutes a new system with spherical symmetry, so the solutions should be represented as  $\phi(r,t)$ , with  $r = |r|$ . At the same time, the radial part of the Laplacian can be expressed as [8]:

$$\nabla^2 \phi(r,R) = \frac{1}{r} \frac{\partial^2}{\partial r^2} r \phi(r,t) \quad (6)$$

In the case of  $r \neq 0$ , there is an auxiliary function  $f(r,t) = r\phi(r,t)$  which respects the homogeneous wave equation with a single spatial variable:

$$\frac{\partial^2 f}{\partial r^2} - \frac{1}{c^2} \frac{\partial^2 f}{\partial t^2} = 0 \quad (7)$$

According to d'Alembert's formula,  $f(r,t)$  represents the sum of two terms depending on  $r \pm ct$ , for which the solution can be written in the form  $f(r,t) = u(t - r/c) + v(t + r/c)$ . After several calculations, for Eq. (1) with the source as Eq. (5) one will obtain [8]:

$$\phi(r,t) = -\frac{q(t - r/c)}{4\pi r} \quad (8)$$

If the substitution  $q(t) = \delta(t)$  is made, will results the function:

$$g(r,t) = -\frac{\delta(t - r/c)}{4\pi r} \quad (9)$$

The wave operator acting on the Eq. (9) gives  $\delta(r)\delta(t)$ , with  $g(r,t)$  as its fundamental solution. Moreover, because for  $t > 0$  the right member of Eq. (9) is equal to zero, one can explicitly add the Heaviside function as a factor. Thus, the basic Green function in infinite space without boundary is obtained by replacing  $r$  with  $|r - R|$  and  $t$  with  $t - \tau$  [8].

In another approach [9], the Green function  $g$  is considered as a solution of the wave equation with an impulsive source function  $\delta$  (i.e. the space-time impulse  $\delta$  is situated in the right member):

$$\frac{\partial^2 g(r,t)}{\partial t^2} - v^2 \nabla^2 g(r,t) = \delta(r,t) \quad (10)$$

where  $v$  is a positive constant.

In practice, the equation for  $g$  can be solved with the aid of the spatial Fourier transform, denoted by  $\mathcal{F}$ , defined as [9]:

$$\mathcal{F}g(r,t) \equiv G(k,t) = \int_{-\infty}^{+\infty} g(r,t) e^{ik \cdot r} dv \quad (11)$$

Starting from the fact that the spatial Fourier transform for  $\partial^2 g / \partial t^2$  is of the form:

$$\mathcal{F} \frac{\partial^2 g}{\partial t^2} = \frac{\partial^2 G}{\partial t^2} \quad (12)$$

and considering the spatial Fourier transform for  $\nabla^2 g$  as  $\mathcal{F}(\nabla^2 g) = k^2 g$  and for  $\delta(r, t)$  as  $\mathcal{F}(\nabla^2 g) = F[\delta(x)\delta(y)\delta(z)\delta(t)] = \delta(t)$ , one will obtain the spatial Fourier transform for Eq. (12) as [9]:

$$\frac{\partial^2 G}{\partial t^2} = v^2(k^2 G) = \delta(t) \quad (13)$$

Due to the fact that in Eq. (12) there are no spatial variable, the partial derivative can be replaced by the total derivative, leading to the following ordinary differential equation:

$$\frac{d^2 G}{dt^2} = v^2(k^2 G) = \delta(t) \quad (14)$$

Since the right member of the Eq. (14) is represented by delta function,  $G$  is considered the Green's function for the ordinary differential equation, whose solutions can be determined by the Laplace transform method [9].

Thus, for  $G_L(k, s)$  as the Laplace transform of  $G(k, t)$ , i.e.

$$G_L(k, s) = \int_0^{\infty} G(k, t) e^{-st} dt \quad (15)$$

for the ordinary differential equation, its Laplace transform will be the algebraic equation

$$s^2 G_L + v^2 k^2 G_L = 1 \quad (16)$$

with  $G_L(k, s) = \frac{1}{s^2 + v^2 k^2}$  as the solution [9].

At the same time, according to the table of the Laplace transform,  $G(k, t) = \frac{\sin vkt}{vk}$ , from

which results that the Green's function for the Eq. (14) is the sinc (Cardinal sine) function.

Based on these considerations, the author [9] states that the inverse Fourier spatial transform of  $G(k, t)$  gives the Green function  $g$  for the 1D wave equation, of the form:

$$g(k, t) = \frac{\theta(vt - r)}{2v} \quad (17)$$

for  $r \geq 0$  and  $t \geq 0$ , with  $\theta$  as the Heaviside function [9].

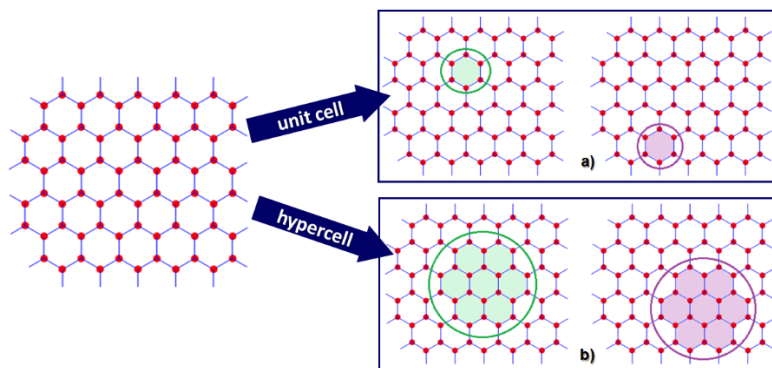
Nevertheless, there are many fields where the Green's function formalism was successfully used, such as statistical, nuclear, solid-state physics, and also in atomic and molecular physics [10]. Green's function can be also used in transport calculation, by solving the problems of single-particle electronic transport, when the density functional Hamiltonian from the Schrodinger equation is used in order to describe the particle energetic [11].

## 2. METHOD

### 2.1. Atomic Cumulative Gradients Model

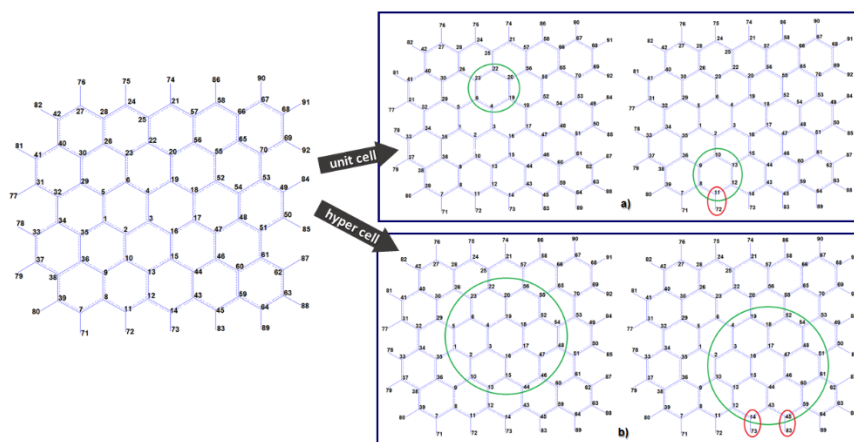
For the present study, the working system consists in a graphene nanoribbon with 25 benzene molecules ( $C_{70}H_{22}$ ) in which one can notice two types of structures – subsystems which can be translated – the smallest, i.e. benzene, generically named unit cell, and a cluster of unit cells, i.e. coronene, generically named hypercell (Figure 2).

**Figure 2:** Graphical representation of the studied system and its corresponding subsystems in monobond and heterobond state. **(a)** Benzene. **(b)** Coronene



The two subsystems form two types of chemical bonds - only with carbon atoms i.e. monobond, and with 1 and 2 hydrogen atoms respectively i.e. heterobond. The aim is to determine how sub-systems energy inside the global system is influenced by the type of bonds created between carbon atoms and hydrogen atoms.

**Figure 3:** Optimized unit cell and hypercell (representation using Hyperchem). **(a)** Benzene. **(b)** Coronene



In order to accurately describe the electronic configuration and the bonds between atoms for the  $C_{70}H_{22}$  molecule it was used the Hyperchem 8.1 program, and geometry optimization

calculations were performed in order to determine its most stable configuration (i.e. in which net forces on each atom are reduced to zero); these calculations are made by adjusting atomic coordinates in steps. As a method of optimization, PM3 semi-empirical method was selected, which describes the electron properties of atoms and molecules by solving the Schrödinger equation with certain approximations. In Hyperchem program, the molecule in study reaches a stable conformation due to the fact that the molecular geometry is altered by energy minimization, leading to lowering the system energy. The minimization progresses by searching the molecular structure in which the energy is not affected by infinitesimal changes in geometry, in other words, the derivative of the energy with respect to all Cartesian coordinates (i.e. the *gradient*) has a value near zero.

## 2.2. Benzene and Coronene Atoms-in-Bonding Gradients

*Single point calculations* were performed on the optimized system, in order to determine the gradient and the total energy for the working system; for this type of calculations, the input molecular structure will show which are the coordinates for a stationary point on the surface of the potential energy. In HyperChem program, the gradient represents the energy rate of change (first derivative) for a molecular system, defined as a function of atomic positions; if its value is very close to zero than the system configuration has minimum energy.

- **Benzene characterization**

From the results obtained with single point, the values representing the atomic gradients for both  $x$  and  $y$  coordinates were selected (see Table 1), for the specific carbon atoms from the unit cell in monobond state (i.e. C<sub>22</sub>, C<sub>20</sub>, C<sub>19</sub>, C<sub>4</sub>, C<sub>6</sub>, C<sub>23</sub>) and heterobond state respectively (i.e. C<sub>10</sub>, C<sub>13</sub>, C<sub>12</sub>, C<sub>11</sub>, C<sub>8</sub>, C<sub>9</sub>).

**Table 1:** Atomic gradients for the unit cell obtained with Hyperchem

BENZENE					
Monobond state			Heterobond state		
Carbon atom	Atomic gradients (kcal/mol/Anstrom)		Carbon atom	Atomic gradients (kcal/mol/Anstrom)	
	x	y		x	y
C <sub>22</sub>	0.03867	-0.01046	C <sub>10</sub>	-0.02062	0.02395
C <sub>20</sub>	-0.03495	0.01800	C <sub>13</sub>	0.03867	0.01046
C <sub>19</sub>	-0.04216	-0.01900	C <sub>12</sub>	0.04206	-0.00817
C <sub>4</sub>	0.04519	0.01768	C <sub>11</sub>	-0.04225	0.00070
C <sub>6</sub>	-0.02502	0.02361	C <sub>8</sub>	0.03036	-0.02978
C <sub>23</sub>	-0.02062	-0.02395	C <sub>9</sub>	-0.01040	0.03250

- **Coronene characterization**

The molecular characterization of the hypercell (in monobond and heterobond states) was made in the same way as for unit cells, the atomic gradients for both  $x$  and  $y$  for the specific carbon atoms being presented in Table 2.

**Table 2:** Atomic gradients for the hypercel obtained with Hyperchem

CORONENE					
Monobond state			Heterobond state		
Carbon atom	Atomic gradients (kcal/mol/Anstrom)		Carbon atom	Atomic gradients (kcal/mol/Anstrom)	
	x	y		x	y
C <sub>22</sub>	0.03867	-0.01046	C <sub>19</sub>	-0.04216	-0.01900
C <sub>20</sub>	-0.03495	0.01800	C <sub>18</sub>	0.01637	-0.02733
C <sub>19</sub>	-0.04216	-0.01900	C <sub>17</sub>	0.01637	0.02733
C <sub>4</sub>	0.04519	0.01768	C <sub>16</sub>	-0.04216	0.01900
C <sub>6</sub>	-0.02502	0.02361	C <sub>3</sub>	0.04519	-0.01768
C <sub>23</sub>	-0.02062	-0.02395	C <sub>4</sub>	0.04519	0.01768
C <sub>56</sub>	0.01424	0.02172	C <sub>52</sub>	0.01455	-0.02717
C <sub>55</sub>	0.01024	0.02590	C <sub>54</sub>	-0.03320	-0.00554
C <sub>52</sub>	0.01455	-0.02717	C <sub>48</sub>	-0.03320	0.00554
C <sub>18</sub>	0.01637	-0.02733	C <sub>47</sub>	0.01455	0.02717
C <sub>54</sub>	-0.03320	-0.00554	C <sub>51</sub>	0.03908	0.00686
C <sub>48</sub>	-0.03320	0.00554	C <sub>61</sub>	0.02427	-0.00592
C <sub>47</sub>	0.01455	0.02717	C <sub>60</sub>	-0.02350	-0.00166
C <sub>17</sub>	0.01637	0.02733	C <sub>46</sub>	0.01024	-0.02590
C <sub>46</sub>	0.01024	-0.02590	C <sub>59</sub>	-0.01654	0.00363
C <sub>44</sub>	0.01424	-0.02172	C <sub>45</sub>	0.00631	0.00374
C <sub>15</sub>	-0.03495	-0.01800	C <sub>43</sub>	0.01519	0.02315
C <sub>16</sub>	-0.04216	0.01900	C <sub>44</sub>	0.01424	-0.02172
C <sub>13</sub>	0.03867	0.01046	C <sub>14</sub>	-0.03637	0.00379
C <sub>10</sub>	-0.02062	0.02395	C <sub>12</sub>	0.04206	-0.00817
C <sub>2</sub>	-0.02502	-0.02361	C <sub>13</sub>	0.03867	0.01046
C <sub>3</sub>	0.04519	-0.01768	C <sub>15</sub>	-0.03495	-0.01800
C <sub>1</sub>	-0.00955	-0.04224	C <sub>10</sub>	-0.02062	0.02395
C <sub>5</sub>	-0.00955	0.04224	C <sub>2</sub>	-0.02502	-0.02361

The atomic gradient values obtained for the selected carbon atoms of unit cell and hypercell (in mono/hetero-bond) were used as input values for calculating the Gradient function, using its algorithm for 1D wave equation from Wolfram Mathematica 11.3 program (see Figure 4).

**Figure 4:** Algorithm for Gradient function for 1D form Wolfram Mathematica 11.3

```

In[*]:= G[x_, y_] := HeavisideTheta[y - Abs[x]]
uG[f_, {x_, y_}] := Integrate[G[y - τ, x - ξ] f[τ, ξ], {τ, 0, y},
{ξ, -Infinity, Infinity}, Assumptions -> x ∈ Reals && y > 0 && τ > 0]
solG = uG[HeavisideTheta[1 - #2] HeavisideTheta[#2 + 1] &, {x, y}]

```

### 3. RESULTS AND DISCUSSIONS

The Heaviside based Gradient function values obtained with Mathematica algorithm for each carbon atom from the unit cell and hypercell are presented in Table 3 and Table 4, and their distribution over the origin is presented in Figure 5 (for benzene) and Figure 6 (for coronene). The total Gradient function was calculated as a sum of the individual values for both cases in each type of bonding.

- **Case 1 - Benzene**

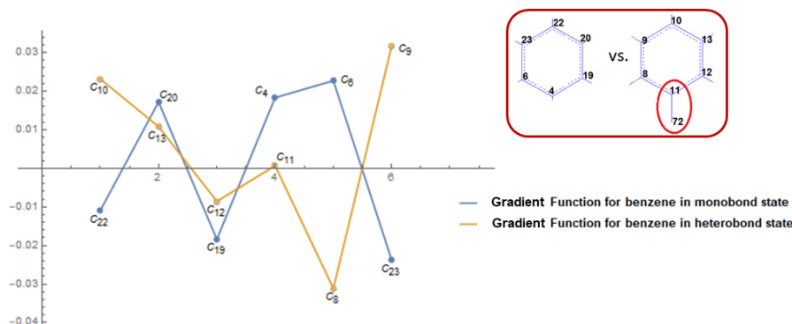
For the unit cell, the results show a difference in the number of positive and negative values between the two bonding states. In monobond state, the negative and positive results are equally distributed over the origin, i.e. the Gradient function values obtained for C<sub>22</sub>, C<sub>19</sub>, and C<sub>23</sub> has negative sign, while the ones for the other three carbon atoms has positive values. However, the positive values are slightly higher than the negative ones; as a result, the total Gradient function value has positive sign and is more close to 0.

On the other hand, in heterobond, only two negative values were obtained, i.e. for C<sub>12</sub> and C<sub>8</sub>, the ones for the other four carbon atoms being with positive sign. For this case, the positive values are even higher than in the previous case, compared to the negative ones; as a result, the total Gradient function value is also positive but more close to 0.1.

**Table 3:** Calculated values of Gradient function for benzen

BENZEN					
Monobond state			Heterobond state		
Carbon atom	Gradient function		Carbon atom	Gradient function	
	C <sub>22</sub>	-0.0109192		C <sub>10</sub>	0.0231693
	C <sub>20</sub>	0.0172089		C <sub>13</sub>	0.0108098
	C <sub>19</sub>	-0.0183795		C <sub>12</sub>	-0.008547
	C <sub>4</sub>	0.0183227		C <sub>11</sub>	0.00067018
	C <sub>6</sub>	0.0227406		C <sub>8</sub>	-0.0311275
	C <sub>23</sub>	-0.023743		C <sub>9</sub>	0.0316339
Total Gradient function					
0.0052305			0.02660868		

**Figure 5:** Gradient function distribution for benzen in monobond vs. heterobond state



- **Case 2 - Coronene**

For the hypercell (i.e. coronene) there is also a difference in the number of positive and negative values between the two bonding states. In monobond, the equal distribution between the negative and the positive results is maintained, same as in benzene monobond i.e. the Gradient function values obtained for C<sub>22</sub>, C<sub>19</sub>, C<sub>23</sub>, C<sub>52</sub>, C<sub>18</sub>, C<sub>54</sub>, C<sub>46</sub>, C<sub>44</sub>, C<sub>15</sub>, C<sub>2</sub>, C<sub>3</sub> and C<sub>1</sub> has negative sign, while the ones for the other twelve carbon atoms has positive value. In this case, the positive values are slightly smaller than the negative ones; as a result, even if the total Gradient function value has negative sign, is still more close to 0.

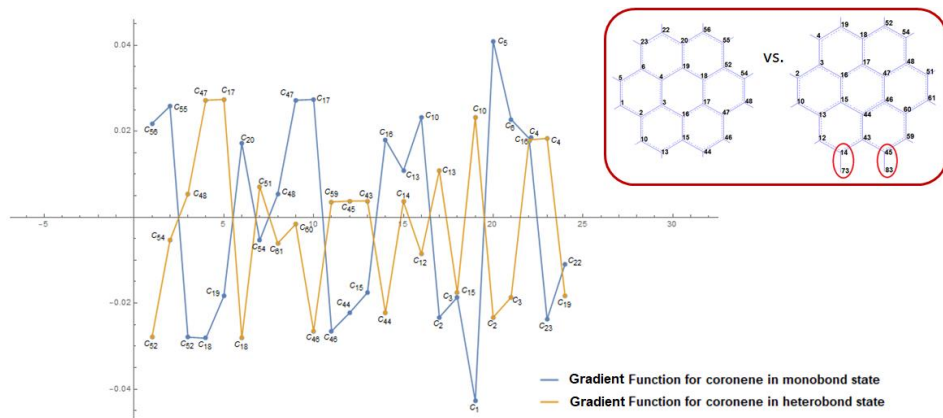
**Table 4:** Calculated values of Gradient function for coronene

CORONENE					
Monobond state			Heterobond state		
Carbon atom	Gradient function		Carbon atom	Gradient function	
	C <sub>22</sub>	-0.0109192		C <sub>19</sub>	-0.0183795
	C <sub>20</sub>	0.0172089		C <sub>18</sub>	-0.0281509
	C <sub>19</sub>	-0.0183795		C <sub>17</sub>	0.0274039
	C <sub>4</sub>	0.0183227		C <sub>16</sub>	0.0180185
	C <sub>6</sub>	0.0227406		C <sub>3</sub>	-0.0186353
	C <sub>23</sub>	-0.023743		C <sub>4</sub>	0.0183227
	C <sub>56</sub>	0.0217934		C <sub>52</sub>	-0.0279344
	C <sub>55</sub>	0.0258298		C <sub>54</sub>	-0.00537142
	C <sub>52</sub>	-0.0279344		C <sub>48</sub>	0.00534073
	C <sub>18</sub>	-0.0281509		C <sub>47</sub>	0.0271962
	C <sub>54</sub>	-0.00537142		C <sub>51</sub>	0.00710456
	C <sub>48</sub>	0.00534073		C <sub>61</sub>	-0.0060812
	C <sub>47</sub>	0.0271962		C <sub>60</sub>	-0.00162237
	C <sub>17</sub>	0.0274039		C <sub>46</sub>	-0.0265006
	C <sub>46</sub>	-0.0265006		C <sub>59</sub>	0.00356337
	C <sub>44</sub>	-0.0222652		C <sub>45</sub>	0.00375661
	C <sub>15</sub>	-0.0175329		C <sub>43</sub>	0.00375661
	C <sub>16</sub>	0.0180185		C <sub>44</sub>	-0.0222652
	C <sub>13</sub>	0.0108098		C <sub>14</sub>	0.00364498
C <sub>10</sub>	0.0231693	C <sub>12</sub>	-0.008547		
C <sub>2</sub>	-0.023298	C <sub>13</sub>	0.0108098		
C <sub>3</sub>	-0.0186353	C <sub>15</sub>	-0.0175329		
C <sub>1</sub>	-0.0427287	C <sub>10</sub>	0.0231693		
C <sub>5</sub>	0.0409445	C <sub>2</sub>	-0.023298		
<b>Global Gradient function</b>			<b>Global Gradient function</b>		
<b>-0.00668079</b>			<b>-0.05223153</b>		

For the second case, in heterobond, the equality between the number of positive and negative values is also maintained, i.e. the Gradient function values obtained for C<sub>19</sub>, C<sub>18</sub>,

$C_3$ ,  $C_{52}$ ,  $C_{54}$ ,  $C_{61}$ ,  $C_{60}$ ,  $C_{46}$ ,  $C_{44}$ ,  $C_{12}$ ,  $C_{15}$  and  $C_2$  has negative sign, the ones for the other twelve carbon atoms being with positive sign. However, the positive values are even smaller than the negative ones, compared to the ones from monobond, this time, the total Gradient function value being with negative sign and more close to  $-0.1$ .

**Figure 6:** Gradient function distribution for coronene in monobond vs. heterobond state



A possible explanation for the difference between the total Gradient function of the benzene bonding states can be the fact that the bond between hydrogen and carbon is stronger than the bond between carbon and carbon. At the same time, the positive value of the total Gradient function can indicate that is more probable for the benzene ring (as a subsystem in the carbon nanoribbon) to become involved in bonds formation with other molecules.

There is also a difference between the two states of coronene, i.e. the global Gradient function for coronene in monobond state is higher than the global Gradient function for coronene in heterobond state, which can be explained by the fact that systems with multiple benzene rings are more stable when bond with other carbon atoms than in the case when bond with hydrogen. At the same time, the negative value of the total Gradient function (different from the positive one obtained for benzene) can also be regarded as a marker of a more stable configuration for coronene as a sub-system of the nanoribbon.

## 4. CONCLUSION

Nowadays, there is still an increased interest in studying graphene due to its applicability in many domains of interest. Recent studies presents graphene as an active material [12] when is used in energy storage mechanisms: it can capture ions (e.g.  $\text{Na}^+$  or  $\text{Li}^+$  ions in ion-metal batteries), can store electrostatic charge (e.g. in double-layer electrochemical capacitors) or it can act as a catalyst (e.g. in metal-air batteries). At the same time, graphene is considered a suitable alternative as an anodic material [13] because it is chemically stable, can exchange electrons easily and has high electrical conductivity, which causes a lower resistive heat inside the electrode (batteries can operate at lower temperatures, being safer). In this context, it is well known in the scientific community that the computational methods are seen as good alternatives to the classical experimental methods, being faster, less expensive and more environmentally friendly, especially when combined with mathematical formalisms. Starting from these

considerations, Gradient function formalism can be seen as a very useful mathematical model in studies of chemistry and physics due to the fact that depends only on the differential operator and the boundary conditions, meaning that it can be easily solved once these conditions are fulfilled. Further connections between the actual Gradient function assessment and the atoms-in-nanostructures Green's functions distribution are to be next studied.

## REFERENCES

1. Savvas, D.; Stefanou, G. Determination of random material properties of graphene sheets with different types of defects. *Composites Part B* **2018**, *143*, 47–54.
2. Mayorov, A.S.; Gorbachev, R.V.; Morozov, S.V.; Britnell, L.; Jalil, R.; Ponomarenko, L.A.; Blake, P.; Novoselov, K.S.; Watanabe, K.; Taniguchi, T.; Geim, A.K. Micrometer-scale ballistic transport in encapsulated graphene at room temperature. *Nano Letters* **2011**, *11*(6), 2396–2399.
3. Balandin, A.A. Thermal properties of graphene and nanostructured carbon materials. *Nature Materials* **2011**, *10*(8), 569–581.
4. Debdeep, J. Graphene. In *Encyclopedia of Nanotechnology, Second Edition*; Bhushan, B. (ed.). Springer Science+Business Media Dordrecht, **2016**, pp. 1346-1357.
5. Han, M.Y., Ozyilmaz, B., Zhang, Y., Kim, P. Energy band-gap engineering of graphene nanoribbons. *Physical Review Letters* **2007**, *98*, 206805.
6. Thouless, D.J., Kirkpatrick, S. Conductivity of the disordered linear chain. *Journal of Physics C: Solid State Physics* **1981**, *14*, 235.
7. Green's Functions in Physics. <https://brilliant.org/wiki/greens-functions-in-physics/>
8. Rastegin, A.E., On elementary derivation of Green's function of wave equation. *Romanian Reports in Physics* **2017**, *69*, 903(1-8).
9. Robinson, E.A., Moser, T.J., Green's Function for the Wave Equation. In *Basic Wave Analysis*. Society of Exploration Geophysicists and the European Association of Geoscientists and Engineers, **2020**, pp. 331–350.
10. Richard, A.R.H.; Feynman, P. *Quantum Mechanics and Path Integrals: Emended Edition*; Publisher: Dover Publications, 2010.
11. Cederbaum, L. S.; Schirmer J. Green's Functions for Open-Shell Atoms and Molecules. *Zeitschrift für Physik* **1974**, *271*, 221-227.
12. Aeberhard, U.; Morf, R.H. Microscopic nonequilibrium theory of quantum well solar cells. *Physical Review B: Condensed Matter and Materials Physics* **2008**, *77*, 125343–125352.
13. Raccichini, R.; Varzi, A.; Passerini, S.; Scrosati B. The role of graphene for electrochemical energy storage. *Nature Materials* **2015**, *14*, 271-279.

Article

## MATRICEAL HETEROJUNCTIONS ON GRAPHENE. FIRST METROLOGICAL MEASUREMENTS

**Doru BUZATU<sup>1</sup>, Paula SVERA (Ianasi)<sup>1,2</sup>, Mihai V. PUTZ<sup>1,2,\*</sup>**

<sup>1</sup>National Institute for Research and Development in Electrochemistry and Condensed Matter, Laboratory of Renewable Energies – Scientific, Str. Prof. Paunescu-Podeanu 144, Timisoara 300569, Romania

<sup>2</sup>West University of Timisoara, Faculty of Chemistry-Biology-Geography, Biology – Chemistry Department, Laboratory of Structural and Computational Physical-Chemistry for Nanosciences and QSAR, Str. Pestalozzi 16A, Timisoara 300115, Romania

### ABSTRACT

Tunable electrical properties of the graphene based materials have huge impact on the current technology expansion, leading to a possibility of multiple improvements of currently used materials, with the potential to develop novel applications. In this study electrical properties of GO/ZnO matrix deposited on ITO glass were investigated.

**Keywords:** graphene, matriceal heterojunctions

### 1. INTRODUCTION

Since its discovery, graphene along with the previously existent carbon allotropes have become part of multiple technologies and composite materials [1]. The properties of graphene include mechanical strength, superior thermal conductivity, transparency, high specific surface area, and excellent charge transport [2,3]. Good conductivity of the graphene can be attributed to the position of p orbitals which result in delocalized  $\pi$  bonds moving freely in the whole graphene plane [4]. As a consequence, high conductivity of graphene could be explained by the presence of zero-energy band gap. More precisely, the place where  $\pi^*$ -state conduction band (CB) and the  $\pi$ -state valence band (VB) touch each other result in Dirac point [5].

Starting from the electronic structure of the graphene, sp<sup>2</sup> hybridization between one s orbital and two p orbitals results in a trigonal planar structure, creating  $\sigma$  bond between carbon

---

\* Correspondent author: mihai.putz@e-uvt.ro

atoms which is adhered to the lattice structure firmness. From this point, unaffected p orbital forms covalent bond with neighboring carbon atoms, resulting in the appearance of  $\pi$  band. Because each p orbital has one extra electron, the  $\pi$  band will be half filled [6].

Introduction of the foreign atoms and defect sites on the lattice of graphene, which highly influence its electrical properties [6,7], is the main cause for the ambivalent nature of the graphene, resulting in a p-type or an n-type semiconductor [8].

A tunable band gap however, could be obtained from insulating to conducting by controlling the reduction degree of rGO, as the band gap energy is strongly correlated with the number of oxidized sites, and the oxidization degree of rGO [9].

The importance of half-filled bands is reflected in large Coulomb energies that cause strong collective effects, magnetism, and insulating behavior of the materials [10]. Taking into account the resonant valence bond structure of the graphene and its semimetal-like behavior, the result is unusual linearly dispersing electronic excitations called Dirac electrons. The importance of the band structure along with the Dirac points is reflected in the graphene properties like high conductivity and electron mobility (Figure 1a and Figure 2) [6,11].

The carrier concentration can be tuned from holes to electrons, which depends of the applied gate voltage, as result having bipolar field effect. Considering the thermal fluctuations, non-uniformities in the material, impurities, electrical charges in the vicinity of graphene, some residual charge carrier concentration may exist in graphene devices [11].

In this work the aim was to study the graphene-oxide/TiO<sub>2</sub> semiconductors with tunable conductivity, placed in a specific matriceal sequence, in order to predict a conductivity pattern based on quantic effects that take place. It is presumed that the non-contact depositions placed at micrometric distances will induce new interactions (Figure 1b).

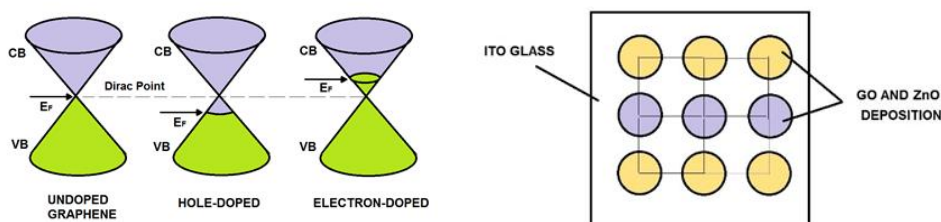


**Figure 1.** a): Dirac point position in case of undoped graphene, hole-doped graphene and electron-doped graphene; b): Matriceal depositions of GO/TiO<sub>2</sub> on ITO glass

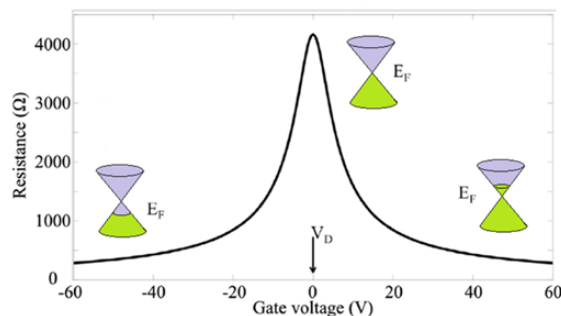


**Figure 2.** Resistance vs Gate voltage dependence for graphene, showing the Dirac point (VD), where resistance reaches a maximum. In this case the Dirac point is at  $VD = 0$  (neutrality point). By applying positive gate voltages, n-doped (electron doped) graphene is made, and vice-versa for p-doped graphene where negative voltages are applied.  $E_F$  marks the Fermi energy [6,11]

## 2. METHOD/MODEL

Quantum mechanics represents an efficient approach for defining accurate and substantial scientific theory [12-15]. Relevant phenomena that occurs in quantum mechanics is superposition and entanglement, that also enables quantum computers to perform, using a variety of physical technologies, such as trapped ions, superconductors or photons. What is common for each approach is the quantum noise, for this reason quantum mechanics states require isolation from the environment. In order to achieve fully functional quantum computers, design of correct algorithms together with error correcting codes is of great importance. In quantum mechanics there are phenomena that are inexistent in classical physics for example the occurrence of two distinct states of the same system [16], whereas the transition between these two states is represented by logical operations. The multiple quantum states are described as qubits when two states are present and qudits when the system number is higher. Because quantum systems can exist simultaneously, a qubit can be either 1 and 0, a property attributed to the superposition. Other advantage is entanglement, a phenomenon which is referred to the dependence between the qubits. Combined together, superposition and entanglement, create main power of quantum computing, named quantum parallelism.

Because qubit's two states are represented in binary information and exist in the same time due to the superposition, the contained information can be described as [12,15]:

$$\alpha |0\rangle + \beta |1\rangle$$

where  $\alpha$  and  $\beta$ , are the complex numbers called amplitudes.  $|0\rangle$  and  $|1\rangle$  are the possible states of the qubit, referred as kets. Using this formula, it can be obtained the quantity of the 0 and 1 provenience of the qubit state. Determination of the qubit state probability is possible with the following formula:

$$\text{prob}(0) = |\alpha|^2$$

$$\text{prob}(1) = |\beta|^2$$

$$|\alpha|^2 + |\beta|^2 = 1$$

Because qubit must be defined in one of the two states, it could be more complicated when  $\alpha$  and  $\beta$  contain negative values or imaginary parts. From this point such attributes allow the occurrence of phase difference between the states  $|0\rangle$  and  $|1\rangle$ . In addition, this notation can be expanded to multiple independent qubits combined, for example:

$$\alpha |0\rangle + \beta |1\rangle \text{ and } \gamma |0\rangle + \delta |1\rangle$$

represented by a tensor product:

$$(\alpha |0\rangle + \beta |1\rangle) \otimes (\gamma |0\rangle + \delta |1\rangle)$$

For entangled states, the following state is suitable:

$$\alpha\gamma |00\rangle + \alpha\delta |01\rangle + \beta\gamma |10\rangle + \beta\delta |11\rangle$$

In the case of entangled states, it is not possible to represent independent qubits, more precisely the quantum state cannot be described by each qubit's specific state, therefore an example of entangled state can be presented as:

$$\alpha |00\rangle + \beta |11\rangle$$

Using Bell's quantum teleportation principle, both qubit states are distinguished by measuring only one of the qubit states. Starting with the previous statement, coefficients for  $|01\rangle$  and  $|10\rangle$  are 0 in case of two qubits, as for final determination, the system must be either in  $|00\rangle$  or  $|11\rangle$  state.

Other important factor in determining the quantum states is the amplitude. The role of the amplitude is to operate as variable of the quantum algorithm, more precisely, in an n qubit system exist  $2^n$  amplitudes. The only disadvantage is that the amplitude cannot be measured directly, whereas when qubits are measured, amplitude is compelled to be either 0 or 1 [12,15].

Because quantum operations overwrite the data in the process, this inconvenience is solved by using approximate computing. Quantum computing is probabilistic by nature; therefore, quantum states are hard to define. Taking into account the existent quantum algorithms (Shor, QFT, Grover, Simon, Deutsch-Josza) approximation algorithms proved to be more suitable highlighting the fact that they can run on near-term, error prone quantum computers [12,17]. In the process, entangled states are directed towards a target state that can minimize a cost function using variation of quantum gate parameters [12, 18].

Other complementary approaches to the quantum algorithms that should be taken into consideration are the error correction and potential for scaling.

In case of quantum computers, the error correction is very important because of the present noise which is also the main reason for the yet inexistent large-scale computers, mainly because the interaction with the environment (or external medium) will damage the quantum state. Because of the fragility that exhibit the existent error correction codes, extra qubits are observed, which have the main goal to interact with the qubits that hold the state.

On the other hand, physical performance of quantum computation implementation is possible using molecular magnets [19], NMR spectroscopy [20], photons [21], non-Abelian anyons [22], trapped ions [23], Quantum Dots [24], and superconductors [12]. Undeniably, for each approach there is a specific system that can describe the process, still there are several conditions that apply to all:

- Quantum information that must exist even in most rudimental state
- Ability to perform a universal family or unitary transformations
- Execution/preparation of a credible and trusted initial state
- Measurement of the resulted output

The first criteria is referred to the necessity for a reliable usage and storage of the information, a property that is extensively used in classical computers. The second item is referred to the universal set that also allows linear transformations. The last two criteria are

related to the classical creation and measurement of states. More precisely, quantum computer should perform arbitrary quantum operations and to have the ability be controlled and measured in a “classical” manner. Still other factors need to be considered, more exactly when evaluating the conditions starting from a physics device, values like coherence time, gate latency, gate fidelity and mobility are crucial, while from an engineering viewpoint, topology (qubit connectivity), maturity, ease of fabrication, control and integration have relevance [12,15].

What is significant in this study is the fact that superconductors rely on the sequence of swap gates in order to move quantum states. Following this direction coupling over long distance superconducting transmission lines could be a new alternative for the superconductors. A milestone in this regard is the fact that superconducting computers have immobile qubits resulting in a better topology involving a better determination of which qubit can interact. At the same time this will have as consequence long distance communication and also swap gates, with a resulting increasing number of required gates. Number of the qubits can determine an increase of gates in the actual system. In comparison to the other existent technologies’ semiconductor and superconductor-based applications are the most appropriate for quantum computers. One example is superconducting computers based on Josephson junctions built with traditional circuit design and produced physically with the aid of lithography [25].

Still after all the benefits of superconductors and semiconductors in quantum computer applications, the existence of reliable physical quantum gates still persists. Quantum technologies use analog signals for operations yet quantum operations are time sensitive, that in consequence can result in delay of pulse on the order of couple nanoseconds which is reflected in an incorrect operation. In addition, superconducting computers require higher number of currents carrying wires which can affect the reliability of the output [12]. This problem was solved by operating at very low temperatures (around 0K) [26]. Due to very demanding conditions of operating at low temperatures and because circuits typically operate at warmer temperature than the qubits, temperature of 4K is more suitable for testing.

### 3. RESULTS

#### 2.1. ZnO and GO matrix deposition on ITO glass

Deposition of GO and ZnO was carried out by drop casting on glass and ITO glass substrate, following a determined matrix pattern as showed in the Figure 3. For the following depositions, one type of ZnO paste and 3 variations of GO were obtained, following two sources of graphene oxide in water dispersia, that were reduced as indicated in preparation of X1, X2 and Y2.

##### 2.1.1. Preparation of ZnO paste

0.4 g of ZnO (purchased from Sigma-Aldrich) was weighted and milled, followed by an addition of 12 drops of water. After mixing the ZnO and water, 0.08 ml of glacial acetic acid was added. After mixing the compounds, 8 drops of triton x 45 were added.

### 2.1.2. Preparation of rGO (X1)

GO (graphene oxide in water dispersion previously obtained by Cataldo et al. [27]) was mixed with 1 mL of 1-ascorbic acid (1M) and left for one hour in the ultrasonic bath at 60 ° C. The mixture was then exposed to a temperature of 90 ° C. 0.45 mL of hydrogen peroxide was then added and the mixture was left for 30 minutes at 60 ° C in the ultrasonic bath.

### 2.1.3. Preparation of rGO (X2)

GO (graphene oxide in water dispersion previously obtained by Cataldo et al. [27]) was mixed with 1 mg of L- ascorbic acid and left for one hour in the ultrasonic bath at 60 ° C.

### 2.1.4. Preparation of rGO (Y2)

GO (commercial graphene oxide in water dispersa purchased from Sigma-Aldrich) was mixed with 1 mg of L- ascorbic acid and left for one hour in the ultrasonic bath at 60 ° C.

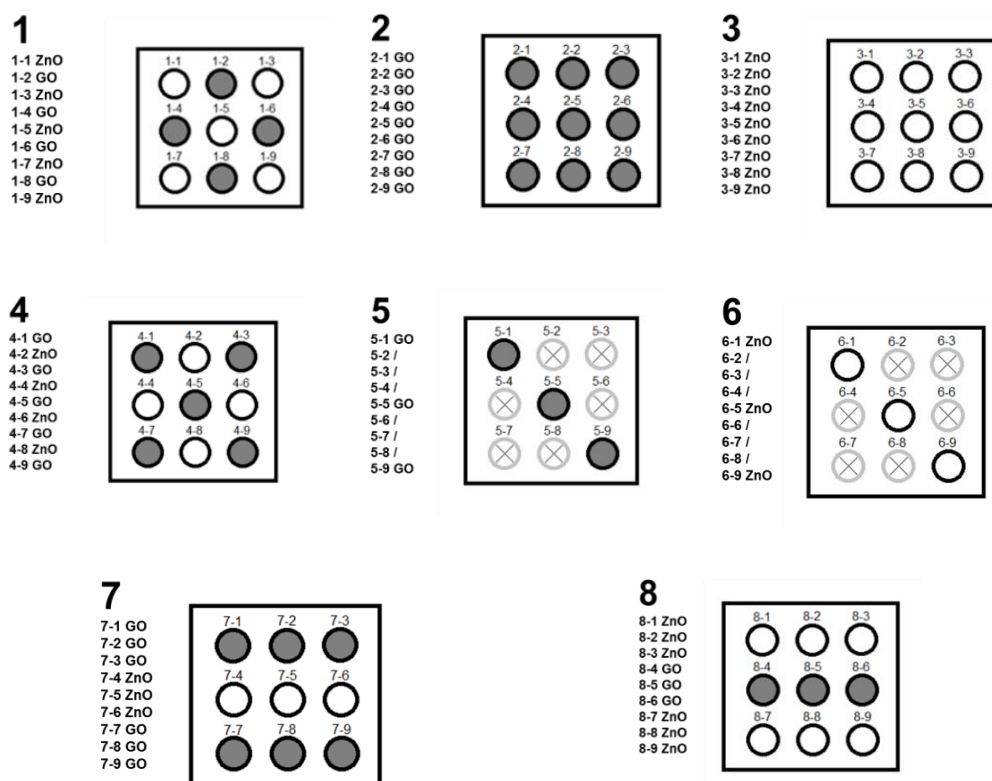
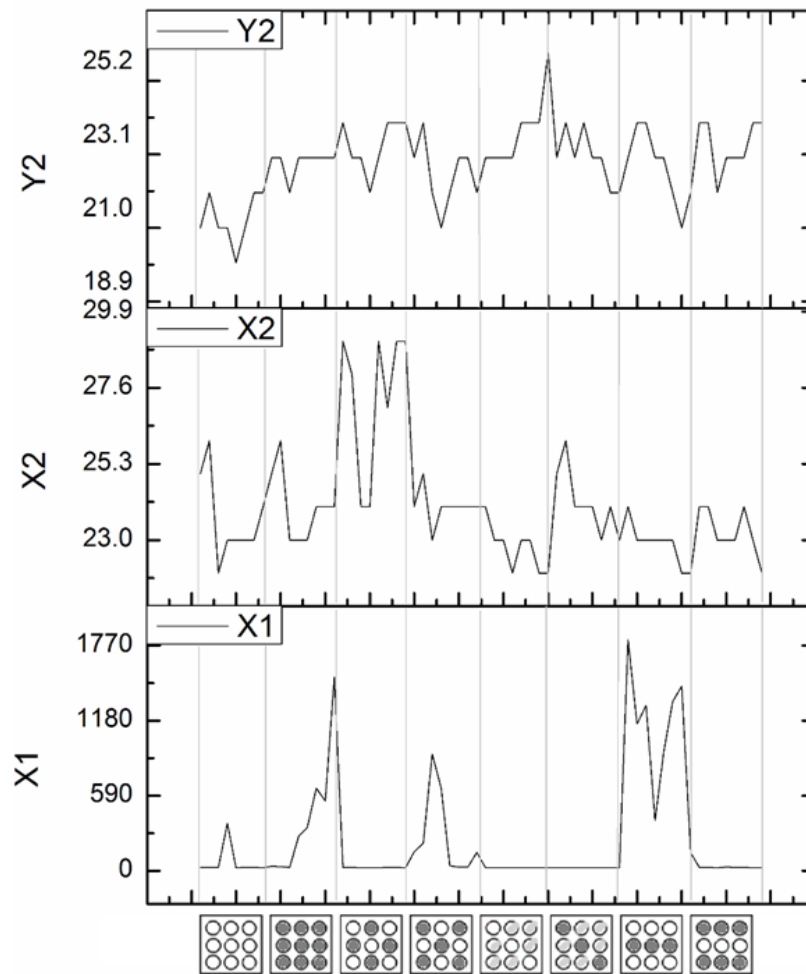


**Figure 3.** Matrix pattern of ZnO and GO deposited on ITO glass: Plate 1; Plate 2; Plate 3; Plate 4; Plate 5; Plate 6; Plate 7; and Plate 8.

2.2. *Electrical resistance, electrical voltage and electric current intensity of the deposited materials (GO/ZnO matrix)*

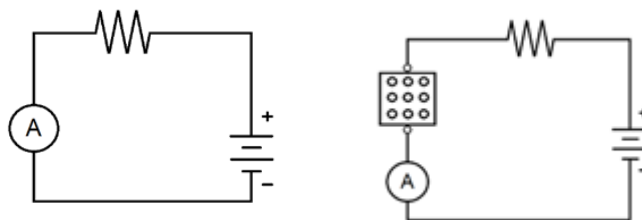
The first electrical resistance measurement was performed on ITO plate. It has been observed that measurements at different distances result in different resistance values. Thereby, measurements were performed at the same distance for all the deposited plates, indicating 20  $\Omega$  for undeposited ITO plate.

Before the electric measurements of the sample, rezistance of each deposition line was checked, indicating high variations in case of X1 (up to 1770  $\Omega$ ), and small variations in case of X2 and Y2 (Figure 4).



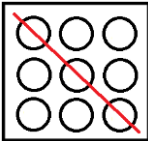
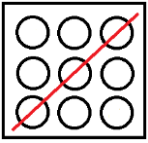
**Figure 4.** Resistance measurements: range and variations of samples X1, X2 and Y2.

Electric measurements were performed with the aid of a multimeter which was connected to a resistance and a battery (Figure 5). In the first phase, U, I and R values were registered in the absence of the deposited plate. With the deposited sample in circuit, no differences in R and U were observed. All in all, the results are presented in Table 1.



**Figure 5.** Circuit scheme: without (left) and with (right) the deposited sample.

**Table 1.** Electric measurements for sample X1, X2 and Y2 at different temperatures (25, 40 and 10°C) and in the presence of a magnet

Measuring area	Deposition number	Current intensity [mA] at 25°C			Current intensity [mA] at 40°C			Current intensity [mA] at 10°C			Current intensity [mA] at 25°C and in presence of magnet		
		X1	X2	Y2	X1	X2	Y2	X1	X2	Y2	X1 m	X2 m	Y2 m
<b>Plate 1</b>													
Values of U, I and R during the entire measurement		1.35 V, 10.1 8 mA, 181 1 Ω	1.33 V, 10.0 9 mA, 172 7 Ω	1.35 V, 10.1 4 mA, 180 0 Ω	1.35 V, 10.2 8 mA, 178 8 Ω at 40° C	1.34 V, 10.1 6 mA, 175 9 Ω at 40° C	1.32 V, 10.2 1 mA, 170 0 Ω at 40° C	1.31 V, 10.1 1 mA, 168 4 Ω at 10° C	1.32 V, 10.1 6 mA, 169 0 Ω at 10° C	1.33 V, 10.1 4 mA, 175 1 Ω at 10° C	1.33 V, 10.0 7 mA, 173 7 Ω	1.33 V, 10.0 9 mA, 172 7 Ω	1.33 V, 10.0 5 mA, 172 7 Ω
	3-1 – 3-9	8.6	0.8- 6	8.6	8.6	0-7	8.6	4- 6.7	6- 8.3	8.5	7- 8.3	1.7- 7.8	8.3
	3-3 – 3-7	8.5	3-8	8.6	8.5	8.5	8.6	0- 6.5	6- 8.2	8.6	6- 8.4	5- 8.2	7- 8.3

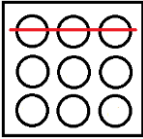
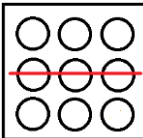
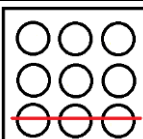
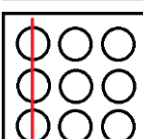
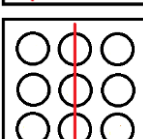
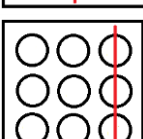
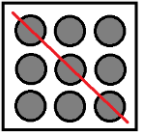
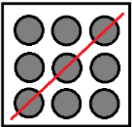
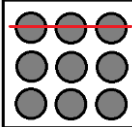
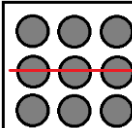
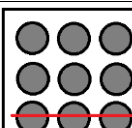
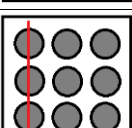
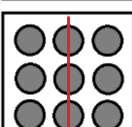
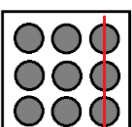
	3-1-3-3	8.6	5-8	8.6	8.7	6.8-8.3	8.6	0-5	6-8.4	8.6	6-8.2	5.5-8.1	8.4
	3-4-3-6	4- <u>8.6</u>	7-8.4	8.6	8.7	0-8	8.6	1-6.4	7.8-8.5	8.7	6-8.4	6.8-8.3	8.5
	3-7-3-9	8.2	0.8-7	8.6	0-8.1	0-6.3	8.7	2-6.7	6-8.3	8.7	6-8.4	5.8-7.3	8.5
	3-1-3-7	8.6	8.2-8.4	8.6	8.6	0-8.4	8.6	7-8.4	8-8.4	8.5	7- <u>8.3</u>	7.6-8.4	6-8.4
	3-2-3-8	8.6	8-8.4	8.6	8.6	6-8.3	8.7	7-8.4	8.2-8.5	8.5	7- <u>8.3</u>	3.2-7.9	8.5
	3-3-3-9	8.6	7.4-8.4	8.7	8.6	6-7.6	8.7	4-8.2	7.8-8.5	8.6	6- <u>8.4</u>	0.1-7.2	8.5

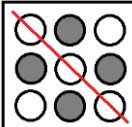
Plate 2

Measuring area	Deposition number	X1	X2	Y2	X1 40	X2 40	Y2 40	X1 10	X2 10	Y2 10	X1 m	X2 m	Y2 m
Values of U, I and R during the entire measurement		1.36	1.33	1.35	1.34	1.34	1.33	1.32	1.32	1.34	1.35	1.33	1.33
		V,	V,	V,	V,	V,	V,	V,	V,	V,	V,	V,	V,
		10.1	10.1	10.1	10.3	10.1	10.2	10.0	10.1	10.1	10.0	10.1	10.0
		8	1	5	3	7	1	3	6	3	5	1	5
		mA,	mA,	mA,	mA,	mA,	mA,	mA,	mA,	mA,	mA,	mA,	mA,
		181	174	180	2Ω	178	175	170	169	169	175	173	174
	8Ω	2Ω	4Ω	at	at	at	at	at	at	at	9Ω	2Ω	9Ω
				40°	40°	40°	at	at	at	10°			
				C	C	C	10°	10°	C				

	2-1-2-9	1.36	8.5	8.6	7-8.2	8.4	8.6	3-7.9	8.2-8.5	8.5	8.5	8.4	8.5
---	---------	------	-----	-----	-------	-----	-----	-------	---------	-----	-----	-----	-----

	2-3 – 2-7	0.2- 7.4	8.5	8.6	1- 7.7	8.5	8.7	5- 7.5	6- 8.2	8.6	8.5	7- 8.3	8.5
	2-1 – 2-3	2- 5.3	8.6	8.7	2- 7.3	8.5	8.8	0-3	8.5- 8.6	8.6	8.6	6- 8.4	8.6
	2-4 – 2-6	0.2- 5.2	6.9- 8.4	8.7	1.9- 5.9	8.5	8.7	7- 8.3	7- 8.4	8.6	8.6	7.9- 8.4	8.6
	2-7 – 2-9	2-8	8.6	8.6	1.2- 4	8.6	8.7	6- 8.2	7- 8.5	8.6	8.5	8.4	8.5
	2-1 – 2-7	6- 8.3	8.6	8.7	8.4- 8.5	8.6	8.7	4- 7.1	8.4- 8.5	8.6	8.5	8.4- 8.5	8.5
	2-2 – 2-8	3-6	8.5	8.8	4- 7.2	8.5	8.7	5- 7.8	0- <u>8.3</u>	8.6	8.6	8.5	8.6
	2-3 – 2-9	0.1- 2	8.6	8.6	5- 7.3	8.5	8.7	0-7	7- 8.6	8.6	8.6	8.6	8.6

## Plate 3

Measuring area	Depositi on number	X1	X2	Y2	X1 40	X2 40	Y2 40	X1 10	X2 10	Y2 10	X1 m	X2 m	Y2 m	
Values of U, I and R during the entire measurement		1.36	1.33	1.35	1.34	1.34	1.33	1.32	1.32	1.34	1.33	1.34	1.34	
		V,	V,	V,	V,	V,	V,	V,	V,	V,	V,	V,	V,	
		10.1	10.1	10.1	10.2	10.1	10.2	10.0	10.1	10.0	10.0	10.1	10.1	
		2	2	2	2	4	1	7	8	9	5	0	4	
		mA,	mA,	mA,	mA,	mA,	mA,	mA,	mA,	mA,	mA,	mA,	mA,	
		184	174	181	6 Ω	6 Ω	4 Ω	4 Ω	4 Ω	4 Ω	2 Ω	173	175	177
		6 Ω	7 Ω	4 Ω	at	0 Ω	4 Ω	9 Ω						
					40°	40°	40°	10°	10°	10°				
					C	C	C	C	C	C				
	1-1 – 1-9	8.5	8.6	8.6	8.6	8.7	8.7	0-7	8.6	8.7	3- 7.4	8.6	8.7	

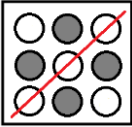
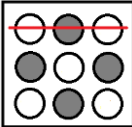
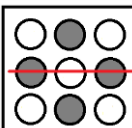
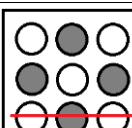
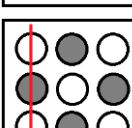
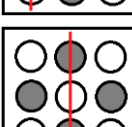
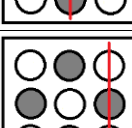
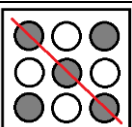
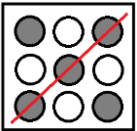
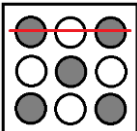
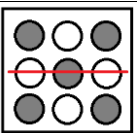
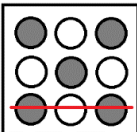
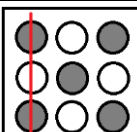
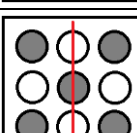
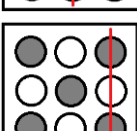
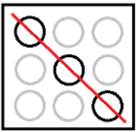
	1-3 - 1-7	7- <u>8.4</u>	8.6	8.6	8.6	8.6	8.7	3-8	8.6	8.6	6- 8.2	8.6	8.6
	1-1 - 1-3	1.9- 8.2	8.6	8.7	4- <u>8.2</u>	8.7	8.8	<u>0-7</u>	8.6	8.6	6- 8.4	8.6	8.7
	1-4 - 1-6	0.4- <u>8.5</u>	8.6	8.7	8.6	8.6	8.8	4- 8.2	8.6	8.7	0- 7.4	8.6	8.7
	1-7 - 1-9	1.6- 8.1	8.6	8.6	8.6	8.7	8.8	0- 7.5	8.6	8.6	5- 8.4	8.6	8.8
	1-1 - 1-7	8.3	8.7	8.7	8.6	8.7	8.7	3.3- 8.2	8.6	8.6	3- 7.8	8.6	8.7
	1-2 - 1-8	4-8	8.7	8.8	8.6	8.7	8.8	7- 8.4	8.6	8.6	6-8	8.6	8.7
	1-3 - 1-9	8.6	8.6	8.6	8.6	8.7	8.8	6.9- 8.2	8.7	8.6	<u>0-4</u>	8.6	8.7

Plate 4

Measuring area	Depositi on number	X1	X2	Y2	X1	X2	Y2	X1	X2	Y2	X1	X2	Y2
Values of U, I and R during the entire measurement		1.35	1.33	1.35	1.34	1.34	1.32	1.31	1.32	1.33	1.33	1.33	1.33
		V,	V,	V,	V,	V,	V,	V,	V,	V,	V,	V,	V,
		10.2	10.0	10.1	10.2	10.2	10.1	10.1	10.1	10.1	10.0	10.0	10.0
		0	4	6	2	0	8	8	7	2	5	4	6
		mA,	mA,	mA,	mA,	mA,	mA,	mA,	mA,	mA,	mA,	mA,	mA,
		180	171	179	177	174	169	168	168	174	172	171	172
		8Ω	8Ω	5Ω	6Ω	6Ω	9Ω	1Ω	0Ω	5Ω	8Ω	8Ω	0Ω
					at	at	at	at	at	at	at		
					40°	40°	40°	10°	10°	10°			
					C	C	C	C	C	C			
	4-1 - 4-9	0-1	8.5	8.6	5- 7.4	5- 7.8	8.7	7- 8.6	6.2- 8.2	8.6	2- 6.2	6.2- 8.1	8.5

	4-3 - 4-7	4-8	7.8- 8.3	8.6	9.3	7- 8.5	8.6	8.4	6.8- 8.2	8.6	7- 8.4	7.8- 8.3	8.6
	4-1 - 4-3	1.4- 5.3	8.2- 8.4	8.7	5.2- 7	4.3- 8.4	8.7	8.6	5.6- 7.6	8.7	0-3	3.6- 7.4	8.5
	4-4 - 4-6	0.6- 7	8.2- 8.3	8.7	4.3- 5.6	6- 8.2	8.7	8.6	4- 7.7	8.6	0-6	2.7- 8	8.6
	4-7 - 4-9	3-7	8.6	8.7	3- 7.7	8.6	8.6	8.4	6- 8.2	8.6	0- 7.6	7.2- 8.4	8.5
	4-1 - 4-7	4- 8.4	8.4	8.7	4.5- 8	8- 8.4	8.7	8.6	8- 8.5	8.7	0- 8.5	5.2- 8.4	8.7
	4-2 - 4-8	0.5- 5	8.5	8.6	5- 8.3	5- 8.5	8.7	8.6	5.3- 8.3	8.6	7- 8.2	5.1- 8.3	8.6
	4-3 - 4-9	1-5	7.3- 8.5	8.7	5- 8.4	8.3	8.7	8.5	6.8- 8.6	8.6	6- 8.2	4.8- 7.4	8.6

## Plate 5

Measuring area	Depositi on number	X1	X2	Y2	X1	X2	Y2	X1	X2	Y2	X1	X2	Y2
					40	40	40	10	10	10	m	m	m
Values of U, I and R during the entire measurement		1.35 V, 10.2 0 mA, 179 1 Ω	1.32 V, 10.1 5 mA, 169 9 Ω	1.34 V, 10.1 4 mA, 178 8 Ω	1.34 V, 10.3 0 mA, 177 0 Ω at 40° C	1.33 V, 10.1 9 mA, 173 0 Ω at 40° C	1.32 V, 10.1 8 mA, 169 3 Ω at 40° C	1.31 V, 10.1 9 mA, 167 2 Ω at 10° C	1.31 V, 10.1 7 mA, 168 0 Ω at 10° C	1.33 V, 10.0 8 mA, 173 2 Ω at 10° C	1.32 V, 10.0 6 mA, 171 5 Ω	1.32 V, 10.1 5 mA, 169 9 Ω	1.33 V, 10.1 7 mA, 170 7 Ω
	6-1 - 6-9	8.6	8.2- 8.4	8.6	8.5	5- 7.5	8.6	8.6	8.1- 8.5	8.6	8.5	4- 8.4	8.6

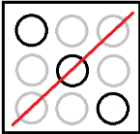
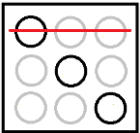
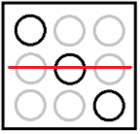
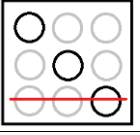
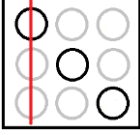
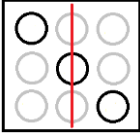
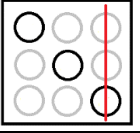
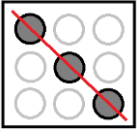
	6-3-6-7	8.8	6.6-8.4	8.6	8.7	5-8.5	8.6	8.6	7.6-8.4	8.6	8.5	0-7.8	8.6
	6-1-6-3	8.7	6.7-8.3	7-8.5	8.7	7-8.6	8.7	8.6	8.3-8.5	8.7	8.5	6.4-8.3	8.7
	6-4-6-6	8.6	7-8.6	6.6-8.4	8.6	8-8.5	8.7	8.6	8-8.5	8.7	8.4	1-8.4	8.6
	6-7-6-9	8.5	2.3-8	8.5	8.6	8.6	8.7	8.6	8.1-8.5	8.6	8.5	7.9-8.5	8.6
	6-1-6-7	8.6	8.1-8.6	8.7	8.7	7.8-8.7	8.7	8.7	7-8.4	8.7	8.5	7.8-8.5	8.6
	6-2-6-8	8.7	7.6-8.5	8.7	8.7	8.5	8.7	8.6	6.8-8.5	8.7	8.6	1-8.4	8.7
	6-3-6-9	8.8	8.6	8.7	8.7	8.5	8.7	8.6	6.6-8.5	8.7	8.5	7-8.6	8.7

Plate 6

Measuring area	Depositi on number	X1	X2	Y2	X1	X2	Y2	X1	X2	Y2	X1	X2	Y2
					40	40	40	10	10	10	m	m	m
Values of U, I and R during the entire measurement		1.35	1.32	1.35	1.34	1.33	1.32	1.31	1.31	1.33	1.33	1.32	1.33
		V,	V,	V,	V,	V,	V,	V,	V,	V,	V,	V,	V,
		10.1	10.0	10.1	10.2	10.1	10.1	10.1	10.1	10.1	10.1	10.0	10.1
		9	7	6	1	9	9	4	7	1	4	6	5
		mA,	mA,	mA,	mA,	mA,	mA,	mA,	mA,	mA,	mA,	mA,	mA,
		179	170	179	2Ω	3Ω	6Ω	5Ω	2Ω	0Ω	172	170	171
		0Ω	5Ω	2Ω	at	at	at	at	at	at	2Ω	1Ω	8Ω
					40°	40°	40°	10°	10°	10°			
					C	C	C	C	C	C			
	5-1-5-9	8.6	8.5	3-6	8.6	8.6	4.8-8.2	8.7	8.7	4-8.2	8.5	8.6	0-6

	5-3-5-7	8.6	8.6	3-7.4	0-6	8.6	3.8-8.4	8.7	8.7	5-8	8.6	8.6	1-6.6
	5-1-5-3	8.7	8.7	4-7.8	8.7	8.7	6-8.3	8.7	8.7	5-8.2	8.5	8.6	1-5
	5-4-5-6	8.8	8.7	3-7.8	8.7	8.7	5-8.3	8.7	8.7	4-8.4	8.6	8.6	1-5.6
	5-7-5-9	8.6	8.7	3.2-7.6	8.7	8.7	8.6	8.7	8.7	5-8.2	8.6	8.6	2-6.6
	5-1-5-7	8.7	8.6	2.3-5	8.6	8.8	6.8-8.4	8.6	8.7	5-8.2	8.7	8.6	0-5
	5-2-5-8	8.6	8.6	0-5	8.8	8.8	5-8.1	8.7	8.7	5-8.4	8.7	8.5	1-6.6
	5-3-5-9	8.8	8.7	2-7.3	8.8	8.7	6-8.2	8.7	8.7	5-8.4	8.7	8.7	1-6

Plate 7

Measuring area	Deposition number	X1	X2	Y2	X1	X2	Y2	X1	X2	Y2	X1	X2	Y2
					40	40	40	10	10	10	m	m	m
Values of U, I and R during the entire measurement		1.35 V, 10.2 mA, 179 0 Ω	1.32 V, 10.1 5 mA, 178 168 8 Ω	1.34 V, 10.1 5 mA, 178 176 1 Ω	1.34 V, 10.1 8 mA, 176 8 Ω	1.33 V, 10.2 0 mA, 171 7 Ω	1.32 V, 10.1 8 mA, 168 6 Ω	1.31 V, 10.1 9 mA, 166 1 Ω	1.31 V, 10.1 8 mA, 167 4 Ω	1.33 V, 10.1 2 mA, 172 6 Ω	1.32 V, 10.0 3 mA, 171 0 Ω	1.32 V, 10.1 5 mA, 168 8 Ω	1.32 V, 10.2 0 mA, 170 4 Ω
					at 40° C	at 40° C	at 40° C	at 10° C	at 10° C	at 10° C			

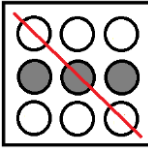
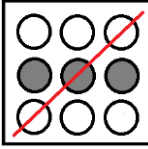
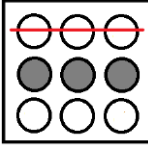
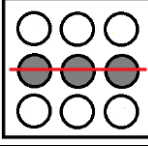
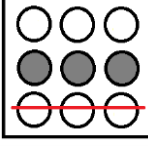
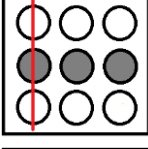
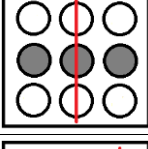
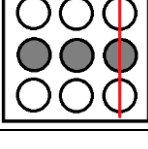
	8-1-8-9	8.6	8.5	8.6	8.6	8.6	8.5	8.5	8.5	8.6	8.3	8.5	8.7
	8-3-8-7	8.6	8.6	8.6	8.4	8.6	8.6	8.5	8.5	8.6	8.5	8.5	8.5
	8-1-8-3	8.7	8.6	8.7	8.6	8.6	8.6	8.6	8.6	8.6	8.5	8.6	8.7
	8-4-8-6	6- 8.7	8.6	8.7	8.6	8.7	8.6	8.5	<u>8.6</u>	8.6	7- <u>8.4</u>	8.5	8.6
	8-7-8-9	4- 6.7	8.5	8.6	8.6	8.6	8.6	8.6	8.6	8.6	4- 8.3	8.5	8.6
	8-1-8-7	8.6	8.6	8.7	8.5	8.7	8.6	8.6	8.6	8.6	8.5	8.6	8.7
	8-2-8-8	8.6	8.6	8.7	8.5	8.7	8.6	8.6	8.6	8.6	6- 8.3	8.6	8.7
	8-3-8-9	8.7	8.6	8.7	8.7	8.7	8.6	8.6	8.7	8.7	8.4	8.6	8.7

Plate 8

Measuring area	Deposition number	X1	X2	Y2	X1 40	X2 40	Y2 40	X1 10	X2 10	Y2 10	X1 m	X2 m	Y2 m
Values of U, I and R during the entire measurement		1.35	1.32	1.34	1.34	1.34	1.32	1.31	1.31	1.33	1.32	1.32	1.33
		V,	V,	V,	V,	V,	V,	V,	V,	V,	V,	V,	V,
		10.2	10.1	10.1	10.3	10.1	10.1	10.1	10.1	10.1	10.1	10.0	10.1
		0	7	6	1	9	8	9	6	2	3	7	5
		mA,	mA,	mA,	mA,	mA,	mA,	mA,	mA,	mA,	mA,	mA,	mA,
		179	169	178	176	174	169	166	167	172	171	169	170
		2 Ω	3 Ω	5 Ω	8 Ω	6 Ω	1 Ω	9 Ω	8 Ω	9 Ω	0 Ω	3 Ω	6 Ω
					at	at	at	at	at	at	at		
					40°	40°	40°	10°	10°	10°			
					C	C	C	C	C	C			

	7-1-7-9	0.7-5	8.7	8.6	0.9-8	8.6	8.6	5-8.2	8.6	8.6	0-3.6	8.6	8.7
	7-3-7-7	2-6	8.5	8.6	8.3	8.6	8.6	8.4	8.6	8.5	0-3.6	8.6	8.6
	7-1-7-3	0.7-5	8.6	8.7	4-5.3	8.6	8.7	8.5	8.6	8.6	0-5.7	8.7	8.6
	7-4-7-6	0-0.8	8.6	8.7	0.6-7.3	8.6	8.6	8.6	8.6	8.6	0-6.8	8.7	8.7
	7-7-7-9	0.2-1.3	8.6	8.7	3-8.6	8.6	8.5	7-8.3	8.7	8.6	0-4.2	8.6	8.6
	7-1-7-7	4-6	8.7	8.7	1.4-8	8.6	8.6	1-7	8.7	8.7	0-3.8	8.7	8.7
	7-2-7-8	0-2	8.7	8.7	0.3-1.3	8.7	8.7	6-8.4	8.8	8.7	0-5.2	8.6	8.6
	7-3-7-9	0-0.3	8.7	8.7	3-7	8.7	8.7	6-8.2	8.6	8.6	0-5.1	8.7	8.6

## 4. CONCLUSIONS

Besides its excellent properties, graphene has also a great potential for detecting the light. Much more important, its ability stands in identifying the light of any color, as a result of fast electronic response, a process described by Tomadin et al. [28]. It was observed that light absorption has an impact on graphene's conductivity, implying both increase and decrease of conductivity. One cause is that in the moment when graphene absorbs light, electrons heat

extremely fast. In case of highly doped graphene, which as a result contains numerous free electrons, electron heating caused by the absorption of light leads to a decreased conduction. On the other hand, weakly doped graphene with less free electrons exhibits increased conductivity due to the formation of free electrons after the light absorption and therefore the created heat positively influences the conductivity of graphene materials.

Furthermore, a desirable feature of any quantum processor is rapid and accurate readout of the qubit states, for this reason most efficient readout technique uses readout resonators coupled to each qubit (circuit QED architecture), although few experimental studies were reported. Among the tested materials are van der Waals multilayered materials (vdW) that include insulators, semiconductors, superconductors and magnetic materials [29]. Wang et al. developed vdW voltage-tunable heterostructures with graphene and semiconductor and observed the appearance of bipolar Josephson current in the ballistic regime. Despite the unusual Dirac band structure formed in graphene, the used qubit configuration facilitated access to electronic gate voltage tuning [30-33].

The present work discusses obtained results of graphene-oxide/ZnO depositions, in 3Qubit configuration, i.e. 8x8 matrix-junction; with the aim to implement various local metal-oxide quantum transistor configurations in future works. More precisely, under applied voltage, the input logical signals (AND, OR, XOR), together with the structural physical-chemical oxides combinations operate as the quantum gate-source-drain connections, so that the obtained quantum transistors produce the 3-qubit outputs, this way developing graphentronic integrated circuits for the use in quantum computing framework.

Adopting the laws of Boolean Algebra, quantum tunneling activation of GO/ZnO depositions is a favorable approach for measuring the logical outcome of the gates. With the aid of quantum Hamiltonian computing (QHC) gate working principle, it is possible to express the quantum level repulsion effect that takes place when stretching the graphenic valence-conduction band gap, as well as the description of quantum interferences that result in synergic tunneling transport [33].

## ACKNOWLEDGEMENT

Authors acknowledge the contribution to this work within the Nucleus-Programme under the project PN-19-22-01-02 and of its 2020 renewal as funded by the Romanian Ministry of Education and Research.

## REFERENCES

1. Pastrana-Martínez, L.M.; Morales-Torres, S.; Figueiredo, J.L.; Faria, J.L.; Silva, A.M.T. Graphene photocatalysts. In *Multifunctional Photocatalytic Materials for Energy*; Woodhead Publishing in Materials volume series, 1st Edition; Lin, Z.; Ye, M.; Wang, M.; Elsevier Science, 2018; pp. 79-101.
2. Novoselov, K.S.; Geim, A.K.; Morozov, S.V.; Jiang, D.; Zhang, Y.; Dubonov, S.V.; Grigorieva, I.V.; Firsov, A.A. Electric field effect in atomically thin carbon films. *Science* 2004, 306:5696, 666-669.
3. Geim, A.K. Graphene: status and prospects. *Science* 2009, 324:5934, 1530-1534.

4. Wang, J.; Ma, F.; Liang, W.; Sun, M. Electrical properties and applications of graphene, hexagonal boron nitride (h-BN), and graphene/h-BN heterostructures. *Materials Today Physics* 2017, 2, 6-34.
5. Avouris, P. Graphene: electronic and photonic properties and devices. *Nano Letters* 2010, 10:11, 4285-4294.
6. Castro Neto, A.H.; Guinea, F.; Peres, N.M.R.; Novoselov, K.S.; Geim, A.K. *Reviews of Modern Physics*. 2009, 81, 109–162.
7. Dissanayake, D.M.N.M.; Eisaman, M.D. Chemical-free n-type and p-type multilayer-graphene transistors. *Applied Physics Letters* 2016, 109, 0531101-0531103.
8. Phan, D.T.; Chung, G.S. P–n junction characteristics of graphene oxide and reduced graphene oxide on n-type Si (111). *Journal of Physics and Chemistry of Solids* 2013, 74:11, 1509-1514.
9. Mathkar, A.; Tozier, D.; Cox, P.; Ong, P.; Galande, C.; Balakrishnan, K.; Reddy, A.L.M.; Ajayan, P.M. Controlled, stepwise reduction and band gap manipulation of graphene oxide. *Journal of Physical Chemistry Letters* 2012, 3:8, 986-991.
10. Phillips, P. Motness. *Annals of Physics* 2006, 321:7, 1634-1650.
11. Lindvall, N. Towards graphene-based devices: Fabrication and characterization, Ph.D. dissertation, Chalmers University of Technology, 2012.
12. Resch, S.; Karpuzcu, U.R. *Quantum Computing: An Overview Across the System Stack* 2019, 1-29.
13. Griffiths, R.B. *Consistent quantum theory*. Cambridge University Press, 2003.
14. Nielsen, M.A.; Chuang, I.L. *Quantum computation and quantum information*, 2000.
15. Wolf, de R. *Quantum Computing: Lecture Notes*, 2019.
16. Jaeger, G. What in the (quantum) world is macroscopic? *American Journal of Physics* 2014, 82:9, 896–905.
17. Aspuru-Guzik, A.; Dutoi, A.D.; Love, P.J.; Head-Gordon, M. Simulated quantum computation of molecular energies. *Science*. 2005, 309:5741, 1704–1707.
18. Wecker, D.; Hastings, M.B.; Troyer, M. Progress towards practical quantum variational algorithms. *Physical Review A* 2015, 92: 4, 042303.
19. Leuenberger M.N, Loss, D. Quantum computing in molecular magnets. *Nature* 2001, 410:6830, 789.
20. Cory, D.G.; Fahmy, A.F.; Havel, T.F. Ensemble quantum computing by nmr spectroscopy. *Proceedings of the National Academy of Sciences* 1997, 94:5, 1634–1639.
21. Milburn, G.J. Photons as qubits. *Physica Scripta*, 2009, T137, 014003.
22. Kitaev, A.Y. Fault-tolerant quantum computation by anyons. *Annals of Physics* 2003, 303:1, 2–30.
23. Cirac J.I.; Zoller, P. Quantum computations with cold trapped ions. *Physical review letters* 1995, 74:20, 4091.
24. Veldhorst, M.; Yang, C.H.; Hwang, J.C.C.; Huang, W.; Dehollain, J.P.; Muhonen, T.; Simmons, S.; Laucht, A.; Hudson, F.E.; Itoh, K.M. A two-qubit logic gate in silicon. *Nature* 2015, 526:7573, 410.
25. Brecht, T.; Pfaff, W.; Wang, C.; Chu, Y.; Frunzio, L.; Devoret, M.H.; Schoelkopf, R.J. Multilayer microwave integrated quantum circuits for scalable quantum computing. *npj Quantum Information* 2016, 2, 16002.

26. DiCarlo, L.; Chow, J.M.; Gambetta, J.M.; Bishop, L.S.; Johnson, B.R.; Schuster, D.I.; Majer, J.; Blais, A.; Frunzio, L.; Girvin, S.M. Demonstration of two-qubit algorithms with a superconducting quantum processor. *Nature* 2009, 460:7252, 240.
27. Cataldo, F.; Putz, M.V.; Ursini, O.; Angelini, G.; Garcia-Hernandez, D.A.; Manchado, A. A new route to graphene starting from heavily ozonized fullerenes: Part 3 – an electron spin resonance study, *Fullerenes, Nanotubes and Carbon Nanostructures* 2016, 24:3, 195-201.
28. Tomadin, A.; Hornett, S.M.; Wang, H.I.; Alexeev, E.M.; Candini, A.; Coletti, C.; Turchinovich, D.; Kläui, M.; Bonn, M.; Koppens, F.H.L.; Hendry, E.; Polini, M.; Tielrooij, K.J. The ultrafast dynamics and conductivity of photoexcited graphene at different Fermi energies, *Science Advances* 2018, 4:5, 5313:1-10.
29. Srivastava, S.; Kino, H.; Joachim, C. Quantum half-adder Boolean logic gate with an nano-graphene molecule and graphene nano-electrodes, *Chemical Physics Letters*, Elsevier 2017, 667, 301-306.
30. Wang, J.I.; Rodan-Legrain, D.; Bretheau, L.; Campbell, D.L.; Kannan, B.; Kim, D.; Kjaergaard, M.; Krantz, P.; Samach, G.O.; Yan, F.; Yoder, J.L.; Watanabe, K.; Taniguchi, T.; Orlando, T.P.; Gustavsson, S.; Jarillo-Herrero, P.; Oliver, W.D. Coherent control of a hybrid superconducting circuit made with graphene-based van der Waals heterostructures, *Nature Nanotech.* 2019, 14, 120–125.
31. Krantz, P.; Kjaergaard, M.; Yan, F.; Orlando, T.P.; Gustavsson, S.; Oliver, W.D. A quantum engineer's guide to superconducting qubits, *Appl. Phys. Rev.* 2019, 6:0213181, 1-57.
32. Namarvar, O.F.; Giraud, O.; Georgeot, B.; Joachim, C. Quantum Hamiltonian Computing protocols for molecular electronics Boolean logic gates, *Quantum Sci. Technol.* 2019, 4:035009, 1-24.
33. Tahan, C. Graphene qubit motivates materials science. *Nature Nanotech.* 2019, 14(2), 102–103.